HIGH TEMPERATURE REFRACTORY-STEEL INTERFACE REACTIONS

DURING MELTING AND CASTING OF HIGH MANGANESE AND

ALUMINUM STEELS AND ELIMINATION

OF PHOSPHORUS PICK-UP

by

Riazur Rahman

A thesis submitted to the Graduate Council of
Texas State University in partial fulfillment
of the requirements for the degree of
Master of Science
with a Major in Technology Management
December 2016

Committee Members:

Anthony S Torres, Chair

Laura N Bartlett, Co-chair

Vedaraman Sriraman

Clois E Powell

COPYRIGHT

By

Riazur Rahman

2016

FAIR USE AND AUTHOR'S PERMISSION STATEMENT

Fair Use

Duplication Permission

ACKNOWLEDGEMENTS

TABLE OF CONTENTS

LIST OF TABLES

LIST OF FIGURES

ABSTRACT

Age hardenable high manganese and aluminum austenitic steels with nominal

composition of Fe-28-30%Mn-6-9%Al-0.6-1%%C-1-1.56%Si-0.5Mo are being

considered as a possible replacement for quenched and tempered Cr and Mo steels

for use in military ballistic armor as well as in the automotive and mining industries.

These steels have an advantage over more traditional high strength steels with up to

18% less density and exceptional combinations of strength and toughness. However

phosphorus is considered as impurity for this steel and should be kept below

0.006%P because of a deleterious effect on toughness. Unfortunately it is very hard

for foundries to achieve these low phosphorus levels, even when extremely pure

charge materials are used.   The source of phosphorus during steelmaking is

unknown and a critical challenge for industrial foundries. Phosphorus containing

monolithic refractory materials have been identified as the possible source of

extraneous phosphorus. Two different experiments were conducted to investigate the

interaction between two different commonly used phosphate and silicate bonded

monolithic refractories and a Fe-Mn-Al-C steel during melting and melt transfer.

The first experiment was designed to study phosphorus pick-up during melting and

long holding times, > 30 min at 1590°C. The second experiment involved short

holding times in a ladle (<30 sec) during melt transfer operations in the foundry.

Laboratory scale experiments showed that these steels can pick-up more than 0.14%

P from phosphate bonded monolithic refractory and this causes heavy grain

boundary k-carbide precipitation and up to 7% of a brittle phosphorus rich eutectic

phase. Whereas steel remelted in contact with silicate bonded refractory showed

almost a 100% austenite matrix and no change in phosphorus content. In the ladle melt transfer operation experiment, negligible increase in phosphorus content and higher Si (0.97%) and C (1.13%) was found in steels poured from phosphate bonded monolithic refractory lined hand-ladle in comparison to silicate bonded monolithic refractory lined hand-ladle poured steels that had Si and C content of 0.74% and 0.97% respectively. Furthermore comparatively higher aged hardening rate and solution treated Charpy V notch, CVN, breaking energy was demonstrated by phosphate bonded monolithic refractory lined hand-ladle poured steels. However regardless of refractory type, aging at 530°C for 10 hours decreased the CVN breaking energy down to an average 5 J. The results of these studies show that dissolved aluminum in molten Fe-Mn-Al-C steels will react with the P2O5 in commonly used refractories that coat the induction furnace and ladles during melting and phosphorus will revert into the melt. The amount of picked up phosphorus is dependent on the processing condition such as holding time. The results of these studies show that phosphorus bonded monolithic refractories should be avoided during melting of Fe-Mn-Al-C steels.

1. INTRODUCTION

For last several decades there has been increasing demand by the military, automotive, aerospace and mining industries for an advanced steel with better structural properties like high toughness, better ductility and reduced weight to increase safety, fuel economy and also to conserve fast depleting natural resources like fossil fuel and metallic elements.[1,2] Keeping that in mind, in late 1950's Ham and Crains started developing steels with composition of Fe-34.4Mn-10.2Al-0.76C that are presently known as advanced high-strength steels (AHSS).[3] Results of that research published in 1958 mentioned that the steel had maximum tensile strength of 730 MPa and 73% elongation to failure ratio, however no information regarding steel treatment process was provided.[3]

Significant research has been recently conducted for the improvement of the mechanical properties of this high manganese and aluminum austenitic steel that typically contains a composition of 15-30 wt.% Mn, 3-12 wt.% Al, 0.3-1.2 wt.% C-0.5-1.50%Si.[2–8] These steels are age hardenable and mechanical properties are thus a function of nano-sized κ-carbide that precipitates in the austenite matrix.   Aging greatly increases the strength but decreases the ductility and toughness. After aging 10 hours at 530°C, it was found that a Fe-30Mn-9Al-1.56Si-0.9C-0.5Mo alloy had hardness and dynamic fracture toughness of 318 ± 14 BHN and 256 ± 66 kJm^{-2}. In comparison, a quenched-tempered 4130 steel showed less toughness of 136 kJm^{-2}.[9]

Fe-Mn-Al-C steels have an austenitic matrix containing no more than 15 vol.% retained ferrite due to the high manganese and carbon content ranging from 20 to 30% Mn and 0.7 to 1.2%C accordingly.[8] Prodhan et al. observed steels with composition of 30%Mn-5.5-9.8%Al-0.27-0.91%C-1.5%Si to contain mostly austenite matrix with

interdendritic ferrite and complex carbide phase in as-cast condition.[10] After solution

treatment at temperatures above 950°C followed by a rapid water quench, steels with

composition of 30%Mn-10%Al-0.9%C contain a 100% austenite matrix.[11] In 2006,

Frommeyer and Brux found that the density decreased by 1.5%/wt.% Al and with the

addition of 12wt.% this resulted in a steel that was18% less dense than quenched and

tempered Cr. And Mo steels.[4] This gives these steels an attractive combination of high

strength and low density.

Phosphorus is considered as an impurity due to its detrimental impact on the

mechanical properties. In 1948, McLean and Northcott reported the embrittlement of the

steel due to phosphorus segregation during solidification and heat treatment.[12] This

segregation not only causes the formation of phosphorus containing brittle eutectic phase

in the interdendritic region but also increases the k-carbide precipitation in the grain

boundary which allows the crack to propagate between the grains easily during an impact

resulting low toughness.[13–15] Phosphorus also decreases the cleavage stress of the k-

carbide up to 45% by creating open volume defects along the <100> direction in the k-

carbide crystal (Fe_3AlC) structure. [16] A drop by 171 J of CVN breaking energy was

recorded at 25°C for Fe-30Mn-9Al-1Si-0.9C steels as the phosphorus increased from

0.001% to 0.07%.[6] In the aged condition, steels with composition of Fe-30Mn-9Al-1Si-

0.9C-0.5Mo showed up to an 80% decrease in CVN toughness from 73 J to 13.6 J at

room temperature when phosphorus content was increased from 0.006 to 0.045%.[16,17]

On the other hand, phosphorus was found to decrease time to reach peak hardness

by promoting formation of k-carbide precipitation that results in increased strength and

hardness.[16] Even though the presence of phosphorus increases the hardness of the high

manganese and aluminum austenitic steel, it severely decreases the toughness and ductility. Thus it is extremely important to keep the phosphorus in high manganese and aluminum steel to below 0.006%. Addition of rare earth material such as cerium and lanthanum to the Fe-30Mn-9Al-1Si-0.9C-0.3Mo alloy during melting helped to reduce phosphorus level but also formed large amount of inclusions which also impacted the toughness of the steel.[18]

Foundries will often use electrolytic manganese and other high purity charge materials to reduce phosphorus levels. However, even this practice of using high purity charge materials in steel making could not prevent the presence of phosphorus up to 0.01% in the melt. Accordingly, in a 2009 study conducted by Howell et al. they surmised that the source of phosphorus in the Fe-Mn-Al-C alloy such as was the refractory materials used to coat ladles.[19] In addition Sutcliffe (2004) mentioned that external sources like refractory, slag or alloying materials can cause formation of various non-metallic inclusions and also determine the several factors like size, chemical composition of inclusion.[20] This research focus on investigation of the factory materials used in Fe-Mn-Al-C steel making process as the possible sources of unwanted deleterious phosphorus.

2. LITERATURE REVIEW

2.1 Background of Fe-Mn-Al-C alloys

In recent years the ultimate goal for many manufacturers is creating a material that has both strong and lightweight properties. These types of materials are not only economically beneficial but also ensure environmental sustainability. In today's transportation industry, The development of advanced lightweight metals with high strength to weight ratios and high energy absorbing capabilities is of extreme importance to the U.S. economy as corporate average fuel economy (CAFE) is ratcheted up to 54 mpg by 2025.[21] In recent years there has also been significant interest in the automotive, energy, military and aerospace industries to develop high energy absorbing materials that are lightweight without sacrificing high strength and toughness. Fully austenitic high manganese and aluminum cast steels containing aluminum, manganese, and carbon as alloying element have excellent combinations of strength and ductility, one type of many different varieties of Advanced High Strength Steel (AHSS).

The light weight Fe-Mn-Al-C alloy actually emerged when Robert Hadfield developed a steel that had increased toughness and exceptional wear resistance containing 13% Mn and 1.2%C in 1882.[22] More than 130 years ago Robert Abbott Hadfield was the 1st person to develop the austenitic manganese steel with the composition of 12.5 % manganese and 1.2 % carbon, which goes under the name of Hadfield Steel.[23]

Back in early 1900s nickel and chromium were used as an alloying element for achieve stainless property in steel. The high price of Cr in the 1980s drove research into

high Al austenitic Mn steels as possible substitutes for Ni-Cr stainless steels.[24–26] To reduce the weight of the metals used in different military applications, U.S Navy developed this alloy steel which eventually became an alternative to the comparatively heavy nickel-chrome stainless steels.[3] The exceptional high strain rate toughness, reduced weight and high work hardening behavior of wrought Fe-Mn-Al-C steels enable to absorb high energy and make it appropriate for the use in automotive industries to improve crash worthiness.[4] Studies in this paper involves steels with nominal composition of 30%Mn-9%Al-0.89-1%C-1-1.56%Si-0.5Mo. When compared to MIL-32269 steels for the use in army battle combat system as amour plate (P900), high manganese and aluminum steels with the above mentioned composition is almost 12-18% lower in density and has similar hardness of 351 HB.[19] This alloy is also considered to use in high strength non-ferromagnetic end rings in generators, ground engaging equipment used in mining industry, body armor for the military vehicles for high impact resistance as substitute for the nickel –chromium stainless steel.

2.2 Role of alloying elements

Most studies of cast Fe-Mn-Al-C steels have centered around a nominal composition of Fe-30%Mn-7-9%Al-0.7-0.9%C-0.5%Mo with varying amounts of Si from 0.5-1.6%. Carbon increases the strength of the Fe-Mn-Al alloy and higher yield strength is achieved with the increase in C content.[27–29] Studies of solution treated followed by water or oil quenched Fe-28-29%Mn-8.5-9.4%Al-C alloy found that 0.8% C gives tensile strength and yield strength of about 850Mpa and 450Mpa respectively which are higher compared to same alloy with 0.6% C that showed 775 MPa tensile strength and 400 MPa yield strength.[27–29] High carbon and aluminum content ranging

from 0.7-1.2% and 9-12% respectively with 28-30% Mn add the property of age hardenability to the alloy by precipitating $E2_1$ perovskite crystal structure k-carbide, $(Fe,Mn)_3AlC$ within the austenitic matrix within temperature range of 350-700°C.[1,4,30–33] James (1969) observed Fe-Mn-Al-C alloy achieve average peak hardness of 410 BHN within temperature range of 550°C to 600°C.[30] Similarly, improvement of yield strength as high as 1016MPa is achievable in Fe-28.8Mn-8.8Al-0.9C-1.4Si-0.5Mo steels upon solution treatment at1050°C for 2 hours and aging at 530°C for 30 hours followed by air cooling.[34]

However over aged Fe-Mn-Al-C alloys containing Si show negative effect on toughness due to promotion of planar slip and de-cohesion of the glide plane forming cleavage fracture by k-carbide precipitation and stimulate B2 or DO3 (5.86 Å) or both intermetallic formation.[7,35,36] High level of manganese near 30% in the alloy helps to achieve stability of austenitic matrix even with lower carbon content and at lower temperature.[11] Reduction in weight without sacrificing mechanical properties is achievable if Al is present at a high amount. It has been found that 1% Al addition causes the of 1.5% density reduction which indicates Fe-Mn-Al-C alloy with up to 12% Al is almost 18% less dense compared to traditional steel.[4] Howell et al. (2008) measured the density of 6.7 g/cm^3 of steels of 30Mn-9Al-1Si-0.9C-0.5Mo composition.[17] Decrease in melting point and increase in fluidity of high manganese and aluminum austenitic steel were obtained by adding silicon, which make the steel production process more sustainable.[36]

It has been suggested in a study that steels that consist of 25-31% Mn, 6.2-9.7% Al and 0.7-1% C demonstrate best balance of impact toughness, ductility and strength.[34]

Mechanical properties of 620 MPa yield strength, tensile strength of 871 MPa and hardness of 272 BHN were reported in a study of 29.4% Mn, 8.8% Al, 1.33% Si and 1% C containing solution treated alloy steels followed by water quenching.[37] Moreover aging at 550°C for 16 hour resulted increase in yield strength, tensile strength and hardness by 264Mpa, 339MPa, 162 BH respectively whereas decreased toughness by 49.6 Jcm^{-2}.[37] However comparatively higher yield strength of 1016 MPa and lower tensile strength of 1085 MPa were reported by Howell et al. (2010) in a study of Fe-28.8%Mn-7.9Al-0.9%C-0.5%Mo0.006%P alloy after being aged for 30 hour at 530°C and work hardening increased it up to 1552 MPa.[34] The above results indicate that improvement of hardness and tensile strength occur at the cost of decrease in impact toughness and ductility upon aging of Fe-Mn-Al-C alloy steels.

Different studies have confirmed that Fe-Mn-Al-C alloy steel is not only 18% lighter than the low alloy high strength steels due to the addition of the aluminum (Al) but also gains 2GPa strength if solution treated and mechanically processed (cold rolled).[4,38] Furthermore, high manganese and aluminum cast steels with the composition of the Fe-30%Mn-9%Al-0.9%C that was solution treated (1050°C for 2 hours), water quenched, and aged for 13 hours at 530C showed up to three times the dynamic fracture toughness of 376 ± 69 kJm^{-2} and 15% less density than normalized, quenched and tempered at 611°C for 1 hour HY-130 martensitic steels with similar strengths.[39] However, it gains more than 80% of true fracture toughness with improved ductility and high range of tensile strength after being solution treated.[4,32]

2.3 Microstructures Dependence on Heat Treatment

According to a study conducted by Howell et al. (2010), the presence of 0.7-1.2% carbon (C) and high manganese (Mn) of 20-30% in this steel helps to retain δ -ferrite phase below 15% and stabilize the austenitic phase under the as cast condition.[34] Microstructures of steels with Fe-30%Mn-9%Al-0.9%C composition in solution treated condition was found to be mixture of austenite and ferrite, however after hominization at 1050°C for 2 hours and followed by water quenching resulted drastic fall in ferrite microstructure with increased volume percentage of austenite matrix.[17] In addition, k-carbide precipitation observed in the grain boundary occurred during slow cooling in as-cast condition was completely dissolved into the austenite matrix.[17] According to phase equilibria developed by Goretskii and Gorev (1990)100% austenitic structure is attainable by solution treatment above 900^0C followed by water quench to 25°C in alloy steels with a composition of 30% Mn, 10% Al and 0.8 to 0.9%C.[11] Typically solution treatment of high manganese and aluminum steels is performed for 2 hours at 1050°C.[11,40,41] According to Frommeyer and Brux (2006) microstructure of TRIPLEX steels with composition of 9-12% Al, 18-28% Mn and 0.7-1.2%C contain mainly γ-austenite, 6-8 vol.% α-ferrite and less than 10 vol.% 20-30nm sized k-carbides. The steels in that study were sequentially solution treated (1050°C for 2 hours), hot rolled (1050°C), annealed (1050°C for 25 min.), cold rolled, recrystallized (1050°C for 25 min.) and finally water quenched.[4]

Chakrabarti and Prodhan (1990) reported relationship between austenitic phase and aluminum – carbon content under both as-cast or homogenized condition at 1100°C.[10] The study reported that ferrite phase of the matrix increases with increase of

aluminum content and decrease of carbon content. With the increase of carbon content from 0.3 to 0.9%, increase in percentage of austenite from 50-100 was found in Fe-30Mn-Al-C alloy, while the aluminum content was kept within 5% to 8%.[42] Most studies have used a 530-550°C ageing temperature with different range of ageing time.[7,34,43] Depending on the aging temperature ranging from 400ºC to 900ºC and alloying elements, Fe-Mn-Al-C alloys may contain various phases like γ-austenite, α-ferrite, κ-carbide, and β-Mn.[30] Various studies reported changes in phase constituents in this alloy during isothermal treatment within the temperature range of 400ºC to 1200ºC.[11,36,41] In solution treated fully austenitic Fe-Mn-Al-C steels, age hardening process promotes carbon depletion of austenite during k-carbide formation leading to ferrite precipitation on the grain boundary with a Kurdjimov-Sachs orientation relationship of $(111)\gamma//(110)\alpha$ and $[10\bar{1}]\gamma // [11\bar{1}]\alpha$.[44,45]

2.4 Impact of Phosphorus on Fe-Mn-Al-A steels

Impurities, even at a small concentration, may significantly affect the mechanical properties of the iron-based alloys. Phosphorus contents as it has been identified as impurity for lightweight high manganese aluminum steels as well as other steels. Recent studies have proved detrimental impact of phosphorus on toughness and ductility even though it increases hardness and yield strength. W. Fordyce back in 1860 first reported about the ability of phosphorus to embrittle the iron at a lower level of 0.5% P.[46] Phosphorous in levels as low as 0.01wt.% can diminish toughness in aged alloys of nominal composition Fe-30Mn-9Al-1Si-0.9C.[18] High phosphorus containing Fe-Mn-Al-C steels above 0.07% were found to contain a hard brittle eutectic phase in interdendritic region that was found to contain high level of phosphorus after EDS mapping.[13,14,18]

Phosphorus segregates on grain boundary during solidification and heat treatment that forms brittle phosphide eutectic on the inter-dendritic region promoting inter-granular brittle fracture and low toughness.[13,47] The models of phosphorus segregation were published by McLean and Northcott in 1948.[12]

According to a study of effect of phosphorus and silicon in Fe-30%Mn-9%Al-0.9%C-0.5 Mo steels by Bartlett et al. (2010) observed decrease in time to peak aging from 60 to 30 hours when phosphorus was present above 0.007% since phosphorus increases the kinetics of Fe_3AlC (κ-carbide) during aging.[48] During the aging process phosphorus enhances both chemical modulation of Al and C that is also known as spinodal decomposition and ordering them into lattice sites simultaneously. This phenomenon results in increase in both size volume fraction of precipitated k-carbide (Fe3AlC) (κ-carbide) manganese and aluminum steels.[6]

Bartlett and Aken (2014) observed increase in hardness and decrease in charpy V-notch (CVN) energy at room temperature in 10 hours aged steel with composition of Fe-30Mn-9Al-1Si-0.9C with the increase of phosphorus content.[6] A study reported increase of phosphorus level from 0.001-0.005% range to more than 0.010 to.015% can significantly reduce CVN energy of Fe-Mn-Al-C system.[15] Other studies reported 80% reduction in charpy V-notch (CVN) energy from 73 Jcm^{-2} to 13.6 Jcm^{-2} at room temperature after increasing phosphorus content from 0.006% to 0.045%.[17,48]

The facture modes in low phosphorus (0.006%) water quenched Fe-Mn-Al-C alloys were found to be a combination of inter-granular and transgranular whereas transgranular cleavage dominated fracture mode in same composition alloys with high phosphorus level of 0.07%.[33,49] Bartlett and Aken (2014) observed transformation of

ductile fracture to low-energy cleavage fracture that resulted reduction of CVN energy from 200J to28 J and increase in harness from 192 BHN to 242BHN in solution treated Fe-30Mn-9Al-0.9C-1Si system when phosphorus level increased slightly from 0.001% to 0.07%.[6]

Furthermore, it was noted that from Fe_3AlC (κ-carbide) structure in Fe-Mn-Al-C alloy aluminum atom gets substituted by phosphorus that causes an open volume defect along the <100> direction.[6,16] As a consequence significant reduction in the cleavage stress as high as 45% of the κ-carbide was observed and is predicted to be the mechanism behind phosphorus decreasing the notch toughness in aged Fe-Mn-Al-C steels.[16] Due to high amount of manganese and aluminum content in Fe-Mn-Al-C alloys, phosphorus cannot be removed effectively during steel making process.[18] Addition of misch metals like cerium and lanthanum were found to be effective in phosphorus removal process from the melt.[18] However Bartlett et al. (2011) observed that process to decrease mechanical properties like ductility and toughness of Fe-Mn-Al-C alloys due to high amount of nonmetallic inclusions.[5] Howell et al. (2010) reported that elimination of phosphorus (0.06%) contained by ferromanganese charge materials from the melt did not result in phosphorus free alloy and chemistry analysis revealed presence of 0.018% phosphorus.[34] Similar kind of result of phosphorus presence was found in various studies that involved use of   high purity electrolytic charge materials which had less than 0.001% phosphorus. Previously possible sources of phosphorus in the Fe-Mn-Al-C were assumed to be crucible material, ladle refractories or   residual material in the furnace from previous heats.[19] Recently Riazur and Bartlett (2015) have observed interaction between molten Fe-Mn-Al-C alloy steels with refractory material and identified

phosphate bonded monolithic refractory as the possible source of phosphorus pick up by the steels.[14] According to that study, thermodynamically dissolution of phosphorus from P_2O_5 in the phosphate bonded refractory to the melt is favorable at steel making temperature of 1590^oC due to the addition of aluminum in the steels with composition of 30Mn-0.81C-9Al-0.53Mo and calculated Gibbs free energy is about -3009 $kJmol^{-1}$.

2.5 Refractories

Under the pressure from users and faced with competition from other materials, steel makers had to propose steel grades with narrower composition ranges, lower guaranteed contents of certain residuals and controlled inclusion size distributions to obtain reproducible service properties. These results can only be reached by a strict control of processes and also of products used during steel making.[50]

The diversification on steel products and their cleanliness requirement in recent years have increased the demand for high quality refractories. Refractory materials have a crucial impact on the cost and quality of steel products as these materials provide good control of chemistry, prevent both formations of non-metallic inclusions and steel surface defects.[51] The physical and chemical properties of refractories play a vital role in obtaining good quality steels. The origin of the word "refractory" is the Latin word "refractarius" which means stubborn.[52] Perhaps it is fitting that refractories used in the steel industry should be stubbornly resistant to high temperatures of the order of 2900^oF as well as chemical attack. Thus refractories are needed to be strong enough to withstand high temperature without undergoing physical or chemical changes while remaining in contact with molten slag, metal and gases. According to American Society for Testing and Materials (ASTM) C71 refractories are non-metallic materials having those chemical

and physical properties that make them applicable for structures, or as components of systems, that are exposed to environments above 1,000 °F (811 K; 538 °C).[53] Some properties of refractory materials include high resistance to temperatures, high-quality mechanical and thermos-mechanical properties like tolerating thermal stress-strain, high resistance to corrosion, erosion and mechanical abrasion, heat buffer between molten metal and the containing vessel walls and conservation of process heat. [52,54–56]

Previous studies showed that external materials like refractories, slag, alloying elements are not only responsible for the formation but also determines the size and composition of inclusion in the steel resulting diminished mechanical properties of steel.[57–62] Evidence of influence on steel purity was found caused by the reaction that took place between refractory lining of ladle and molten steel while treating it in ladle.[20] Extensive research has been conducted to understand the various mechanisms at play in the systems. Oxidation reactions between refractory oxides and metallic elements, refractory dissociation, volatilization, direct dissolution of the refractory with or without precipitation, combination of the refractory and a non-dissolved existing inclusion in the steel are some of the possible mechanisms of steel quality degradation caused by refractories.[51] The amount of dissolution that is cause of corrosion/erosion of refractory materials into slag and molten steels is dependent on the processing temperature, holding time and rotation time as well as nature of chemical bond of refractory.[20,63] A concentration gradient occurs while molten steel, slag come in contact with refractory boundary thus components of refractory diffuse through the interfacial film that and dissolve in the molten steels.[54] The dissolution rate of refractory elements are observed to

be directly related to the concentration gradient between molten steels and refractory boundary.[54]

Currently different types of refractories also known as "industrial ceramic" of wide variety of complex microstructures and phase aggregation are commercially found in the market and each type is engineered and manufactured in a manner that is appropriate for specific application.[52,56,64,65] Most commonly found refractories are oxide based materials, however recently developed refractories are complex in nature which contains non-oxide components like metallic particles, graphite, SiC and resin etc.[52,56,64] Four different types of bonds such as temperature dependent hydraulic bond and organic bond, ceramic bond with hardening by sintering during firing and chemical bond formed due to chemical reaction are observed in refractories in general.[54] Rigaud and Landy (1996) mentioned that ISO classifies refractory materials in 4 categories, such as basic, non-basic, oxide-carbon and specialized materials as shown in figure 1.1.[66]
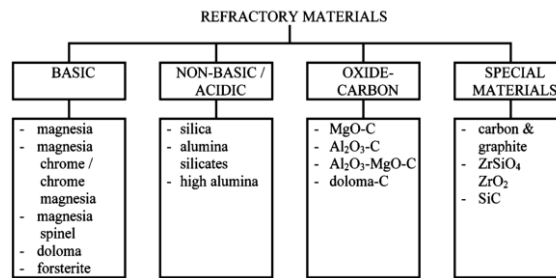
Figure 1.1: Classification of refractory materials [66]

Furthermore depending on the fabrication form, refractories can be classified as shaped and non-shaped (monolithic) refractories, where shaped refractories include fired and unfired materials with predetermined shapes, precast shapes and fusion cast refractories.[67] In addition, plastic mixes, castables, ramming materials, dry vibratables, gunning materials, fettling materials, coatings and mortars are examples of non-shaped or

monolithic refractories. Monolithic refractories are most popular in induction melting process for forming spout of the furnace, capping lip of the ladle and coating inner wall of the transfer ladle etc. since monolithic or unshaped refractories are easy to install, easily available, consume less energy resulting reduced downtime as well as labor cost in comparison to shaped brick installation.[14,63,68]

The initial strength of monolithic refractory develops during installation or forming process. The final strength is achieved when exposed to high temperature during steel making process.[54,63] Currently there are various kinds of monolithic refractories based on methods of use in variety of application are available namely plastic, rammable, castable, pumpable, injectable, gunning, dry vibratory, mortars, coating refractory etc.[54,63] Both pump-able and castable refractories are in dry form and mixed with water or other solvent prior to application. Plastic and ramming refractory come in premixed form and pneumatic rammer or mallet is used for installation process to consolidate to proper density. Mortars and coating refractories are generally found in dry and slurry form respectively, however appropriate consistency required for specific application is very important. For gunning mixes, the dry granular or palletized material should have good adhesion to the gunned surface, low rebound, and appropriate properties as designed to be installed using gunning equipment.

Among various type of monolithic refractories, aluminum industries are using phosphate bonded monolithic refractory for decades that binds ingredients together.[68] At elevated temperature phosphate binder develops strong bonds in monolithic ramming mixes and also participate in ceramic bond formation.[69] In addition this also provides certain resistance to wetting that occur due to corrosive metal and slag. In comparison to

shaped phosphate bonded bricks, these refractories have lower hot strengths due to relatively high liquid content and lower wear resistance.[68] High manganese and aluminum steel making foundries extensively uses plastic rammable monolithic refractory to cap the induction furnace, form the pouring spout, coat the inner surface of the transfer ladle. Kuang et al. (2000) mentioned that during steel making process, these is strong possibility of chemical reaction between refractory and molten metal and physical erosion of the refractory.[70] Furthermore Sutcliffe (2004) reported that during the ladling operation, reaction between refractory and the molten steel can produce detrimental inclusions that reduces the steel purity.[20] In addition the chemistry, amount and size of the inclusions are directly influenced by the steel, refectory composition.[20] Thus it has been reported that, high manganese and aluminum steels can pick up external phosphorus from the phosphate bonded plastic monolithic refractory materials during steel pouring and ladle transfer operation in induction steel making process.[14]

3. STEEL REFRACTORY INTERACTIONS AND ELIMINATION OF PHOSPHORUS PICKUP IN HIGH MANGANESE AND ALUMINUM STEELS

R. Rahman[1] and L.N. Bartlett[2]

[1,2]Texas State University, San Marcos, TX

3.1 Abstract

Fully austenitic high manganese and aluminum cast steels are up to 18% less dense than quenched and tempered Cr and Mo steels, with comparable strengths and up to seven times the dynamic fracture toughness. However, the presence of phosphorus in levels greater than about 0.006 wt.% has a detrimental impact on ductility and toughness. Previous studies have shown that phosphorus pickup of up to 0.02 wt.% P is possible even when high purity charge materials are used and this may be the effect of phosphorus leaching from phosphate bonded refractories during melting and pouring. The current study investigates the interaction between two commercially available refractories and a high manganese and aluminum steel during melting and casting. Two revert samples of chemistry Fe-30Mn-9Al-1.6Si-0.9C-0.5Mo (0.002%P) were melted under protective atmosphere in a high purity alumina crucible lined with phosphate and silicate bonded refractories, respectively. After solidification, specimens were sectioned for chemical and microstructural analysis. Melting in contact with the phosphate bonded refractory resulted in significant phosphorous pickup in the steel of more than 0.14 wt.%P. However, the steel melted in contact with the silicate bonded refractory showed little reaction with the refractory with a phosphorous content of 0.001 wt.%. Microstructural analysis utilizing optical and scanning electron microscopy with EDS showed heavy phosphorus segregation on grain boundaries in the specimen melted in contact with the phosphate bonded refractory which stabilized a high amount of grain boundary κ-carbide precipitation and up to 7% of a brittle phosphorous rich eutectic phase.   The steel melted in contact with the silicate bonded refractory consisted of an austenitic matrix with up to 1% ferrite, showed no evidence of the phosphorous eutectic, and less carbide

precipitation on grain boundaries. The results show that phosphorous pickup can be

significant when phosphate bonded refractories are used and these refractories should be

avoided when melting Fe-Mn-Al-C steels.

3.2 Introduction

During the last decade there has been much research in the development of advanced high strength steels (AHSS) with reduced density for use in high energy absorbing applications in the military and automotive industry. Fully austenitic high manganese and aluminum steels, or Fe-Mn-Al-C alloy steels, are up to 18% less dense than low alloy high strength steels with strengths up to 2 GPa in the solution treated and cold rolled condition.[1,2] Considering cast steels, there has been much research based on the Fe-30%Mn-9%Al-0.9%C composition, which is almost 15% less dense than cast quenched and tempered martensitic steels with similar strengths and up to three times the dynamic fracture toughness.[3] Unless specified otherwise, all compositions in the following text are expressed in terms of weight percent. Mechanical properties in these steels are a function of age hardening and steel cleanliness. Aging in the temperature range of 350 to 700° C greatly increases both hardness and strength by the homogeneous precipitation of κ-carbide, $(Fe,Mn)_3AlC$, within the austenite matrix.[4,5] A study by Howell et al. of a Fe-29Mn-8Al-1.4Si-0.9C-0.5Mo steel showed an increase in tensile strength from 766 to 1085 MPa after aging for 30 hrs at 530°C.[6] However, ductility and toughness are reduced with increased aging and Bartlett et al. recorded a loss in dynamic fracture toughness from 700 kJ/m^2 in a solution treated Fe-30Mn-9Al-1.6Si-0.9C-0.5Mo steel to 144 kJ/m^2 after aging 40 hrs at 530°C.[7]

Recent studies have proved that different types of impurities in the Fe-Mm-Al-C alloy steels have a negative impact on important mechanical properties. In particular, phosphorus in Fe-Mn-Al-C alloy steels increases the strength and hardness during aging but severely decreases both ductility and toughness. According to Bartlett et, al. less time

is required to reach peak hardness if the phosphorus content is high in the Fe-Mn-Al-C alloy system.[8] In that study, Fe-Mn-Al-C alloy steels containing greater than 0.007% phosphorus demonstrated time to peak hardness of about 30 hours while steels with less than 0.007% P took up to 60 hrs to fully harden. Thus, phosphorus increases the kinetics of κ-carbide precipitation during aging. Additionally, an increase in phosphorus content above about 0.006%P severely lowers the Charpy V-Notch impact toughness in the solution treated and aged steels.[7] A study by Howell et al. showed a sharp decrease in the room temperature CVN energy of an aged Fe-30Mn-9Al-1Si-0.9C steel, from 73 J/cm^2 to 13.6 J/cm^2, as the P content increased from 0.006 % to 0.043%.[9] Likewise, an increase of phosphorus from 0.0001% to 0.07% drastically refractories, a phosphate bonded refractory and a silicate bonded refractory, to identify and eliminate the source of phosphorus inclusion in Fe-Mn-Al-C alloy steel.

3.3 Experimental Procedure

The steel used in this experiment was re-melted from a commercially cast high manganese and aluminum steel plate casting with a composition of   Fe-30Mn-9Al-1.56Si-0.9C-0.5Mo and with low phosphorus content, 0.002%P. The chemistries of the steels were determined by optical emission arc spectroscopy and by ion coupled plasma spectrometry after sample dissolution in perchloric acid. Two 92g samples were prepared for re-melting to study interface reactions and phosphorus pickup from two commercial available refractories. An image of the specimens is shown in Figure 3.1.
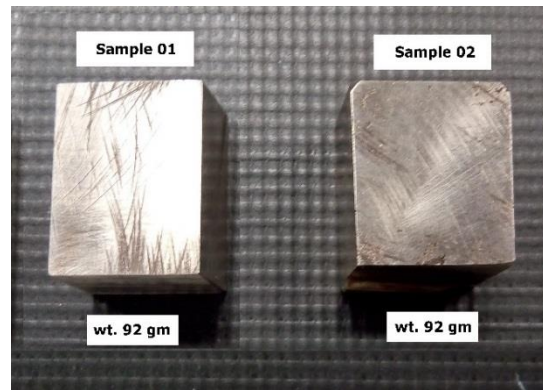
Figure 3.1**:** The low phosphorous steel specimens before re-melting.

Two alumina crucibles were lined with the refractories and allowed to air set prior to the placing the sample specimens in the crucibles. The inner surface of one ceramic crucible was coated with phosphate bonded 90 RAM PC Plastic Monolithic refractory (Figure 3.2 a) with the composition of 15-25wt.% Al_2SiO_5, 75-90wt.% Al_2O_3 ,0.1-1wt.% H_3PO_4, 0.1-1wt.% SiO2 . The inner surface of other crucible was coated with D11NP refractory as shown in Figure 3.2 (b). The D11NP contained no phosphate binder and was composed of pure alumina bonded with 10wt.% Na_2SiO_3. The maximum performance temperature of both refractories was 1700°C. Both were allowed to thoroughly cure prior to use.

Table 3.1: Chemistry of the as-received commercially cast steel in weight percent

Fe	Mn	Al	C	S	Si	Mo	Cu	Ni	P
Bal.	29.97	8.81	0.89		1.56	0.53	0.006	0.007	0.002

The space in between the two crucibles was partially filled with pure carbon powder to prevent the oxidation of the alloy steel samples and create a localized reducing atmosphere. A pure alumina ceramic lid was put on top of the smaller refractory lined crucible as well as the top of the outer crucible. Each assembly was placed inside of a box furnace and heated at a rate of 8°C per minute to 1590°C and then held for 30 minutes.

(a)   (b)
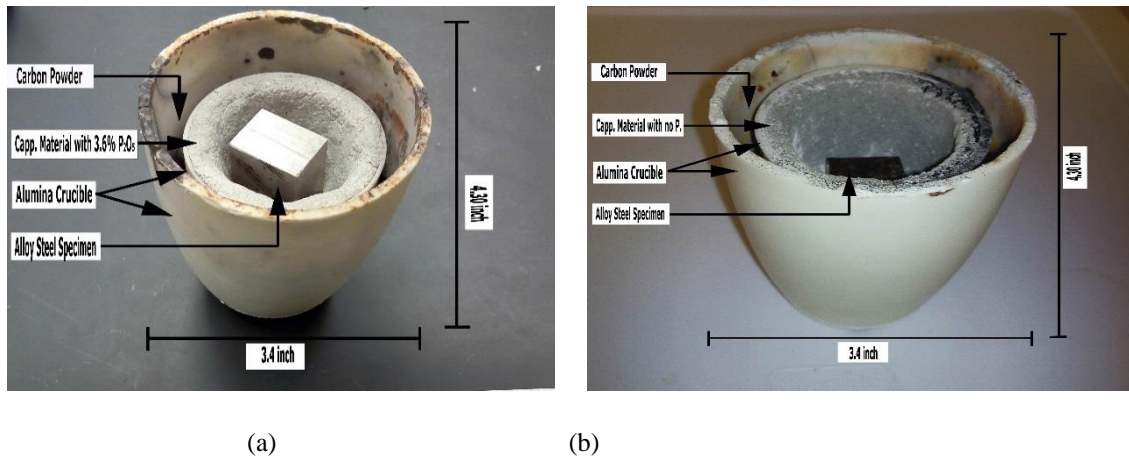
Figure 3.2: The 92 gram samples of steel was re-melted in a double walled alumina crucible. The inner crucible was lined with (a) a phosphate bonded alumina refractory commonly used to cap the crucible and form the pouring spout of induction furnaces and ladles and (b) a silicate bonded alumina refractory castable. Coarse carbon powder was poured in void between the crucibles to create a localized reducing atmosphere.

The specimens were then cooled at a rate of 10°C per minute. A protective argon atmosphere was maintained in the furnace chamber at a flow rate of 20 SCFM. The resulting re-melted and solidified specimens were removed from the crucibles and sectioned for analysis using a water cooled abrasive saw. The chemical composition of the re-melted alloy steel sample was measured using optical emission arc spectroscopy. Sections were polished from each specimen using standard metallographic techniques for

analysis of the microstructure. The surface microstructures of the both un-etched and etched specimens were observed using optical methods at different magnification levels using a Nikon Epiphot 300 optical microscope. Etching was done using 5% Nital. Analysis and measurement of the chemistry of different microstructures on the surface of the etched and un-etched specimens were carried out by using an FEI field emission scanning electron microscope (SEM) equipped with energy dispersive x-Ray spectroscopy (EDS).

3.4 Results

3.4.1 Optical inspection and chemical analysis

Figure 3.3 shows the re-melted specimens after withdrawal from the furnace. Optical observation confirmed that both specimens had fully re-melted during the experiment. Figure 3.3 (a) shows the steel specimen that was re-melted in contact with the phosphorus containing refractory. It shows a small amount of a white crystalline phase has formed along surface at the interface between the refractory and the steel. A scanning electron image of this phase is given in Figure 3.4. It is shown that this phase is acicular in nature and is most consistent with alumina (corundum), Al_2O_3. A small amount of alumina was also found on the surface of the steel that was melted on the silicate bonded refractory. However, it should be noted that the amount of alumina that formed was a very small amount and the re-melted specimens were otherwise free of oxides. Figure 3.3 (b) shows the steel that was melted in contact with the silicate bonded refractory.
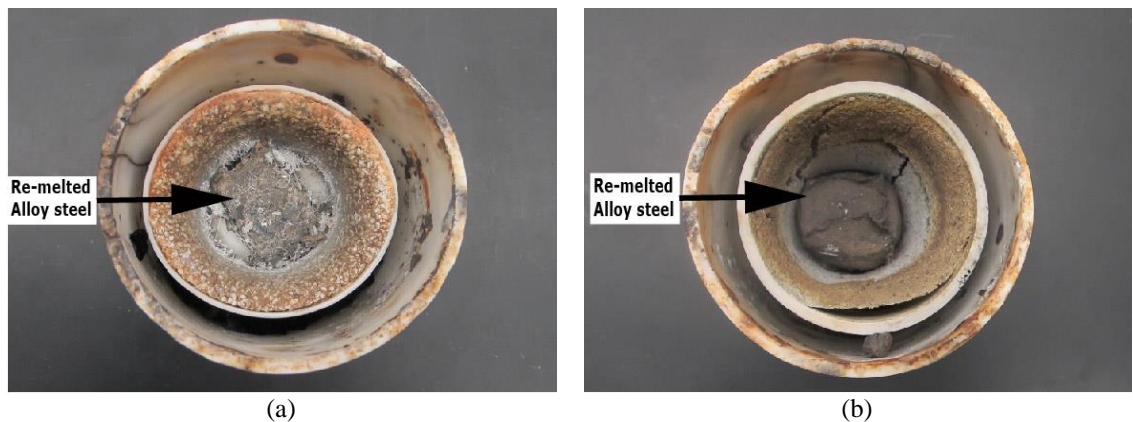
Figure 3.3: The steel specimens after melting in contact with the (a) phosphate bonded refractory and (b) the silicate bonded refractory. (a) A small amount of crystalline oxide was shown to have formed on the surface of the steel that was in contact with the refractory

The re-melted specimen was easily removed and little interaction between the steel sample and the silicate bonded refractory was observed as shown in Figure 3.3 (b).

In contrast, the steel seemed to wet the surface of the phosphate bonded refractory and was more difficult to remove.   This indicates possible reaction between the steel and the phosphate bonded refractory. Specimens were then sectioned and chemical analysis was preformed via optical emission arc spectroscopy. The chemistry of both re-melted specimens in comparison to the original chemistry of the steel is shown in Table 3.2. The chemical analysis shows that the as-received sample had chemical composition of about 0.002 wt. % phosphorus and roughly 30 and 9 wt.% of Mn and Al, respectively.

(a)   (b)
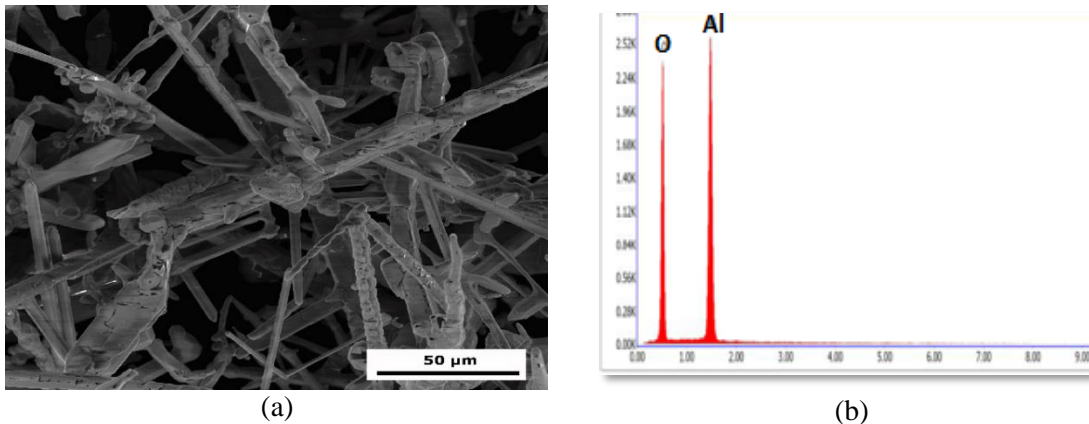
Figure 3.4: (a) A scanning electron image of the crystalline oxide that formed on the surface of the steel and at the interface with the phosphate bonded refractory shows that it is hexagonal and acicular in nature. (b) The corresponding EDS spectrum shows that it is hexagonal and acicular in nature. (b) The corresponding EDS spectrum shows that this phase is crystalline alumina.

After re-melting on the phosphate bonded refractory, the steel absorbed a surprising amount of phosphorus, of more than 0.14%P. This indicates that there was a significant interaction between the P containing refractory and the sample while re-melting. On the contrary, no significant change in amount of phosphorous was found for the alloy steel specimen that was re-melted in contact with the silicate bonded refractory and Table 3.2 shows that the phosphorous content is similar to the original composition at 0.001%P. In addition, it is shown that there is significant increase in the amount of silicon when the steel was re-melted in contact with the phosphate bonded refractory. The silicon level was found to increase from 1.56%Si to 2.58% Si and the amount of

aluminum decreased from 8.81% Al to 7.11% Al when the steel was melted in contact

with the phosphorus containing refractory. In contrast, there was very little change in the

chemistry of the steel when re-melted against the silicate bonded refractory (Table 3.2).

Table 3.2: Chemical analysis of as-received steel in comparison to the re-melted steels

Specimens	Fe	Mn	Al	C	Si	Mo	Cu	Ni	P	Ti	S
As-received Steel	Bal.	29.97	8.81	0.89	1.56	0.53	0.006	0.007	0.002	_	_
Re-melted on P-refractory	Bal.	30.64	7.11	1.14	2.58	0.57	0.009	0.006	>0.14	0.017	0.034
Re-melted on silicate refractory	Bal.	29.95	8.42	0.96	1.78	0.53	0.009	0.006	0.001	0.017	0.019

3.4.2 Microstructural analysis

Figure 3.5 shows the optical micrographs of the as-received steel after sectioning

and polishing. The optical micrograph of the as-received steel in Figure 3.5 shows a

microstructure of nearly 100% austenite with small volume percentage of ferrite islands.

Austenite grain boundaries are shown after etching and this is indicative of κ-carbide

precipitation on grain boundaries as shown in Figure 3.5.

(a)   (b)
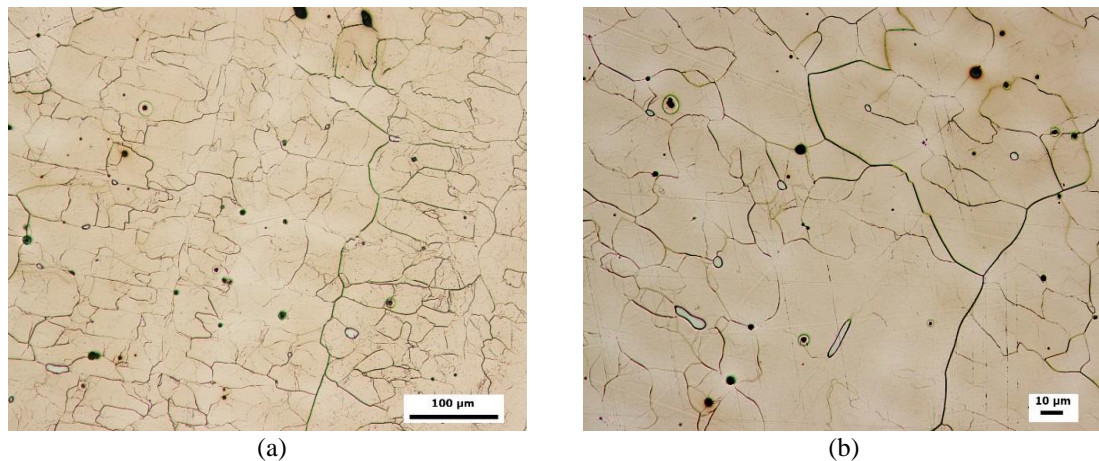
Figure 3.5: Optical micrographs of the as-received commercially cast Fe-30Mn-9Al-1.56Si-0.9C steel with
0.002% P. The specimens were etched with 5% Nital and show a microstructure of many austenite with less
than 1% primary ferrite islands. Grain boundaries are highlighted by κ-carbide precipitation.

The optical micrographs of the un-etched re-melted specimens are shown in

Figure 3.6. A small amount of grain boundary precipitation is noted in the steel specimen

that was re-melted in contact with the silicate bonded refractory as shown in Figure 3.6 (a). In comparison, the steel that was re-melted in contact with the phosphate containing refractory shows significant areas of an interdendritic eutectic phase, up to 7%, as shown in Figure 3.6 (b). Etching outlined the grain boundaries and revealed other microstructures in the steel specimens as shown in Figure 3.7. The steel melted against the silicate bonded refractory has an as-cast microstructure of nearly 100% austenite with small islands of less than 1% ferrite as shown in Figure 3.7 (a and b). Grain boundaries are outlined with carbide precipitation. A second phase precipitate, perhaps an alloy carbide or an intermetallic phase has precipitated at the interface between the austenite and the ferrite and is shown to grow in preferred directions within the ferrite grains (Figure 3.7 a and b). Figure 3.7 (c and d) shows the as-solidified and etched microstructure of the steel that was melted in contact with the phosphate containing refractory. A significant amount of the hard interdendritic eutectic phase is noted to coat grain boundaries.

All specimens in Figure 3.7 were etched using the same concentration of nital and for approximately the same amount of time, however, the phosphorus containing steel specimen shows a significant difference in the level of contrast between interdendritic areas and the center of austenite grains as shown in Figure 3.7 (c and d). This indicates significant alloy segregation. Isolated ferrite was not observed in the phosphorus containing steel regardless of the high phosphorus and silicon levels (Table 3.2). Precipitation of coarse cellular κ-carbide was also observed on grain boundaries of the high phosphorus steel, as shown in Figure 3.7 (c and d). In addition, the high phosphorus steel contained a great deal of matrix carbide or intermetallic precipitation.

28

Some second phase matrix precipitation was also noted in the low phosphorus specimen, but precipitation in the high phosphorus specimen was much more coarse and widespread as shown in Figure 3.7.

<div align="center">(a)   (b)</div>
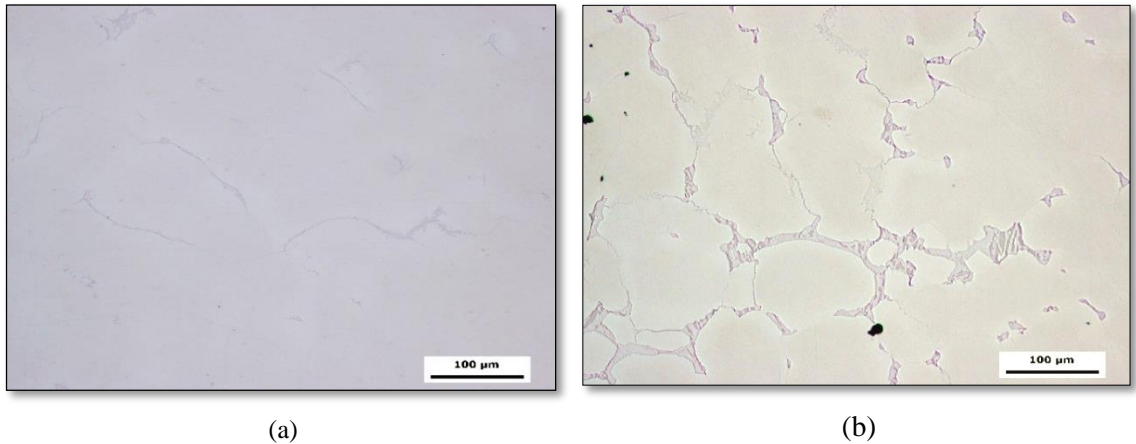
Figure 3.6: The un-etched optical micrographs show (a) some areas of grain boundary precipitation consistent with a carbide or intermetallic phase in the as-solidified steel that was melted on the silicate refractory. (b) The microstructure of the steel that was melted in contact with the phosphorous containing refractory shows widespread formation of a two phase eutectic in interdendritic regions.

The scanning electron images of the low phosphorus and high phosphorus steels are shown in Figures 3.8 (a) and (b), respectively. The low phosphorus specimen shows matrix austenite with areas of continuous precipitation on grain boundaries in addition to isolated areas of ferrite. The high phosphorus specimen shows large areas of the interdendritic eutectic phase and cellular precipitation of carbide on grain boundaries (Figure 3.8 (b). The eutectic is shown to be globular in some areas and to coat grain boundaries in other areas and this is most likely due to the wetting of grain boundaries during slow cooling. The eutectic phase was often accompanied by the presence of both continuous and lamellar carbide on grain boundaries as shown in Figure 3.8 (b).

<div align="center">(a)   (b)</div>

<div align="center">(c)   (d)</div>
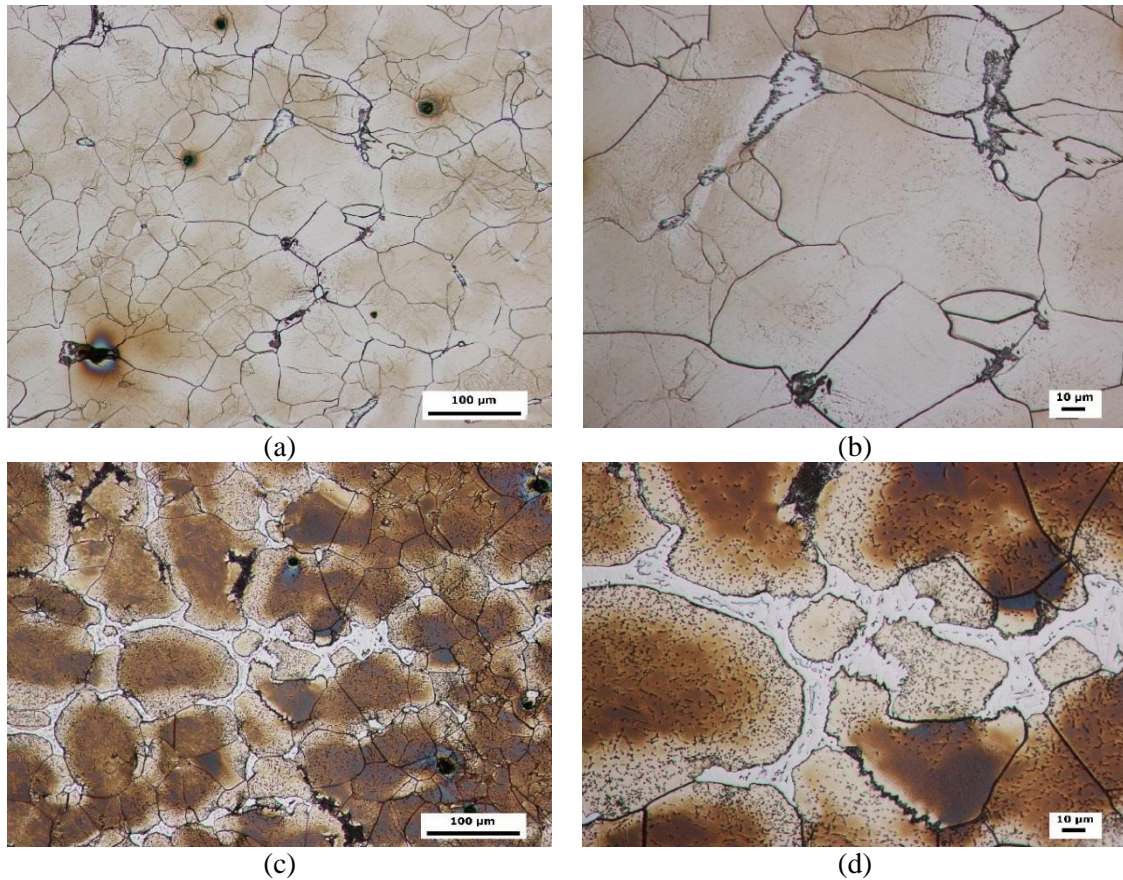
Figure 3.7: The optical micrographs of the as-solidified steel that was re-melted in contact with the (a and b) silicate bonded refractory and (c and d) the phosphate bonded refractory. Specimens have been etched with 5% Nital. (a and b) The low phosphorus steel is nearly 100% austenite with less than 1% ferrite. (b and d) Cellular precipitation of carbide on austenite grain boundaries is observed in both steels but is most prevalent in the high phosphorus steel. (c and d) A large amount of a hard eutectic phase is shown in interdentritic regions of the high phosphorus steel.

3.4.3 EDS analysis of microstructures

The chemistry of the different phases noted in the as-cast structures of both steels was determined by semi-quantitative EDS analysis. Figure 3.9 (a) shows a grain boundary triple point in the as-solidified low phosphorous steel. The EDS spectrum of the continuous grain boundary precipitation in Figure 3.9 (a) is shown in Figure 3.9 (b) and is high in Al and C when compared to the matrix austenite and thus the continuous precipitation is most consistent with κ-carbide. A ferrite grain is shown in the bottom of Figure 3.9(a) to have a plate-like phase that has precipitated on the ferrite-austenite grain boundary and has grown into the ferrite.

<div align="center">30</div>

(a)   (b)
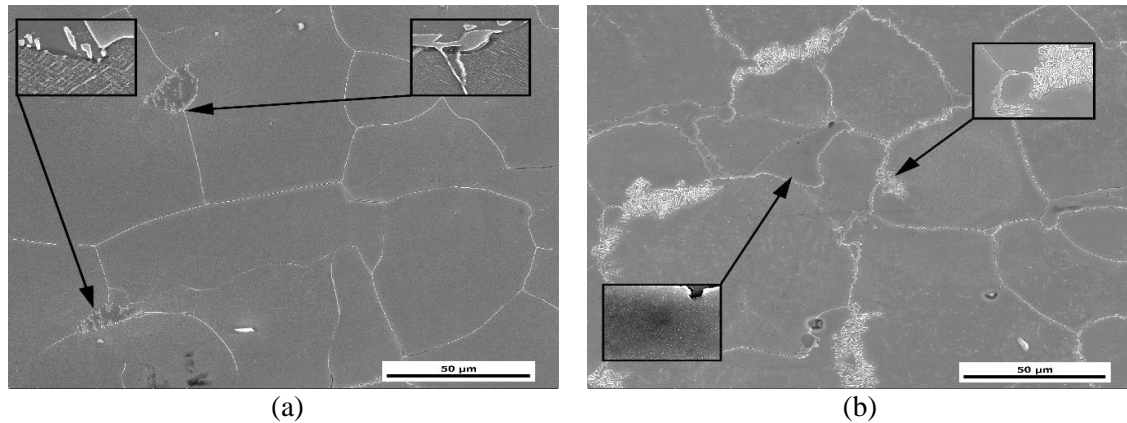
Figure 3.8: Scanning electron images of the as-solidified low phosphorus steel (a) and the high phosphorus steel (b). (a) The low P steel consists of an austenitic matrix with continuous precipitation on grain boundaries and isolated islands of ferrite (inset image). (a) The inset image shows that there is some second phase precipitation that has nucleated at the austenite – ferrite interface and grown into the ferrite. (b) Large areas > 50µm of a hard and brittle eutectic phase were widespread in interdendritic areas (bottom inset image). Large areas consistent with cellular carbide precipitation are shown on grain boundaries (top inset image).

EDS chemical analysis of this phase is shown in Table 3.3. Results show that this phase is rich in C and Al in comparison to the ferrite phase and this is most consistent with κ-carbide. Mn and Si showed a tendency to segregate to the ferrite. Continuous grain boundary precipitation of κ-carbide on austenite grains was significantly lower in Al but richer in C compared to the κ-carbide that grew in contact with the ferrite, see Table 3.3. Large matrix κ-carbide plates were noted to have homogenously precipitated and coarsened along austenite <100> directions as shown in Figure 3.9 (a). The plates were typically 500 to 700 nm in length and around 90 nm thick. Matrix precipitation κ-carbide was especially prevalent in areas around ferrite islands as shown in Figure 3.9 (a) and this suggests that carbon was partitioned from the ferrite to the austenite during cooling making those local areas richer in carbon and stabilizing a greater amount of κ-carbide. Unfortunately, the composition of matrix κ-carbide in these samples could not be determined. Figure 3.9 (c) shows an area of blocky as well as a lamellar type carbide that was noted to precipitate on austenite grain boundaries during solid state cooling in the low phosphorous steel. It should be noted that the occurrence of this phase on grain

31

boundaries was not widespread in the microstructure. The EDS spectrum for this area is given in Figure 3.9 (d) and shows that this phase is rich in C, Mn, and Mo. Table 3.3 shows that the chemistry of these lamellar carbides is consistent with that of an M3C type alloy carbide.

(a)   (b)

(c)   (d)
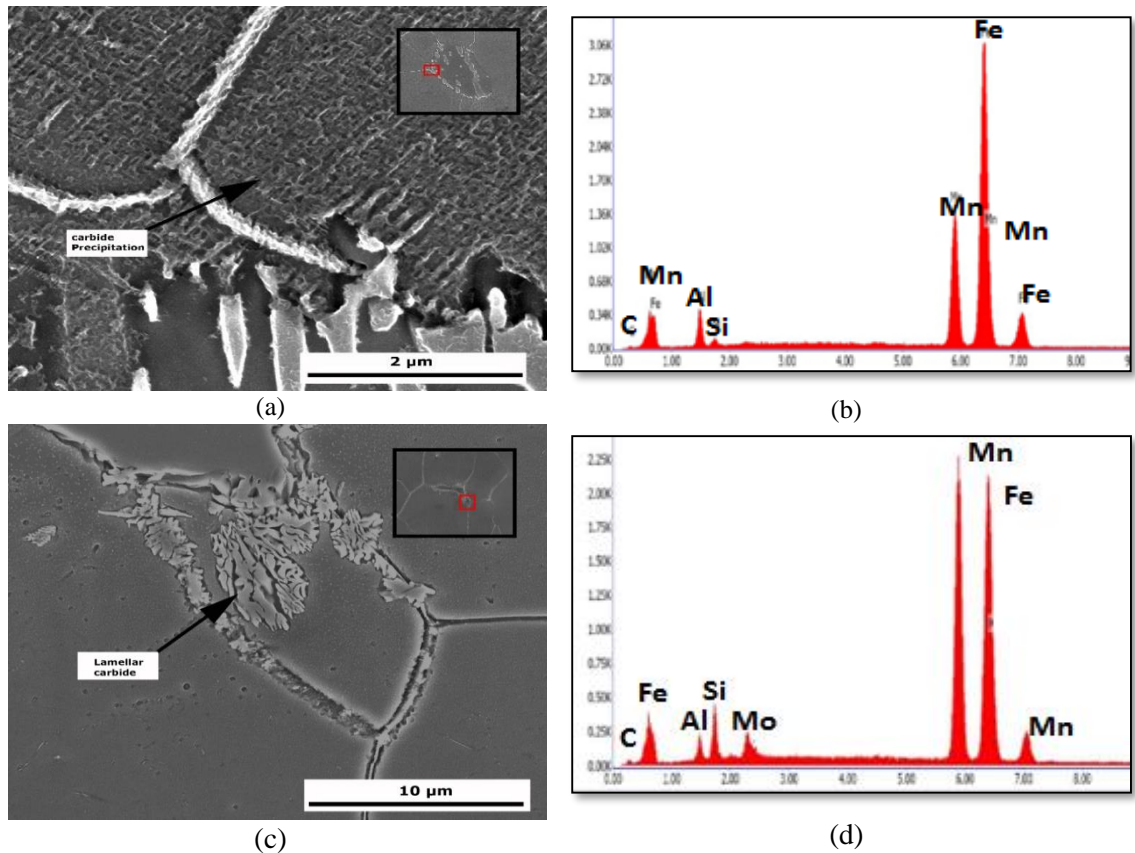
Figure 3.9: Microstructures and corresponding EDS spectra found in the as-solidified low phosphorus specimen. (a) An austenite grain boundary triple point shows continuous grain boundary precipitation that is consistent with κ-carbide precipitation as shown in (b). The area at the bottom of (a) is a ferrite grain in which plate-like κ-carbide has precipitated and grown from the austenite-ferrite grain boundary. (c and d) Some grain boundaries were covered with a eutectic alloy carbide that was found to be rich in Mn, Mo, and Si.

The high magnification SEM images of micro-constituents present in the high phosphorus steel are shown in Figure 3.10. The eutectic phase previously noted in Figures 3.7 (d) and 1.8 (b) is shown on an austenite grain boundary in Figure (3.10) a. This phase appears to be very brittle and is shown to have fractured during the sectioning and polishing process as shown in Figure 3.10 (a). The EDS spectrum of this phase is

shown in Figure 3.10 (b) to be rich in P, Mn, Mo, Si, and C. Therefore inspection of

Figure 3.10 (a) shows what appears to be a binary eutectic of iron-manganese phosphide

and austenite. However, in some regions a ternary phosphide eutectic was observed that

is similar to ternary eutectic steadite in cast iron.

Table 3.3: EDS chemistries of micro-constituents (in atomic percent) observed in the low phosphorus specimen

Phase	Fe	Mn	Al	C	Si	Mo	P
Austenite matrix	47.5	25.3	11.1	13.8	1.13	-	-
Ferrite	61.6	22.9	14.1	-	1.38	-	-
Grain boundary κ-carbide	43.5	17.2	13.8	24.4	1.30	-	-
K-carbide in contact with ferrite	44.0	17.95	17.0	20.0	1.16	-	-
Lamellar alloy carbide	33.4	32.2	4.61	20.2	7.86	1.67	-

This ternary phosphide was found to be most consistent with an iron-manganese

phosphide matrix with globular regions that were found to be slightly higher in

phosphorus, as well as areas of austenite. Figure 3.10 (c and d) show an area of a ternary

phosphide. The high phosphorus regions are shown as globular islands. Cellular carbide

was noted to precipitate on grain boundaries in the high phosphorus steel in juxtaposition

with the phosphide eutectic as shown in Figure 3.10 (a) and 10 (e). The EDS spectrum of

one of these areas of cellular carbide is shown in Figure 3.10 (f) and is rich in Al and C,

which is most consistent with κ-carbide. Table 3.4 gives the EDS chemistries of all of

the major phases noted in the as-solidified high phosphorus steel. The phosphide eutectic

is shown rich in Mn, P, Mo, Si, and C but depleted in Al when compared with the matrix

austenite.
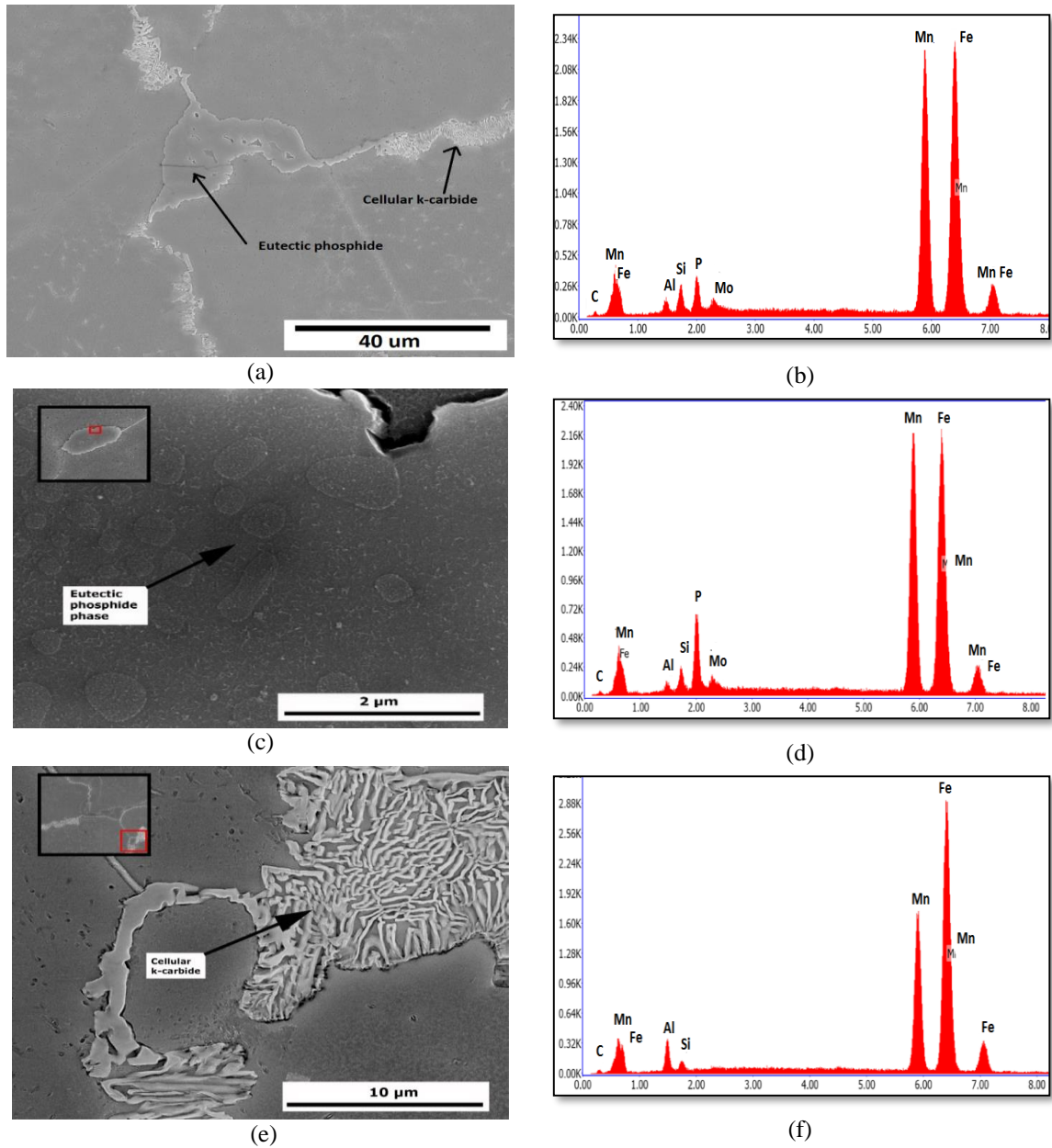
Figure 3.10: The microstructure of the as-solidified high P steel consisted primary austenite with 7-10% of a hard and brittle interdendritic eutectic phosphide phase (a and c) that is rich in P, Mo, Mn, and Si (b and d). (a and e) Austenite grain boundaries were covered with cellular eutectoid carbide that is high in C and Al and is most consistent with κ-carbide as shown in (f).

Table 3.4: EDS chemistries of micro-constituents (in atomic percent) observed in the high phosphorus specimen

phase	Fe	Mn	Al	C	Si	Mo	P
Austenite matrix	57.6	31.7	3.8	5.21	1.62	-	-
Cellular κ-carbide	54.7	27.5	5.1	11.4	1.39	-	-
Phosphide eutectic	45.6	39.7	1.6	6.11	2.40	0.55	4.01

3.5 Discussion

Knowledge of high temperature reactions that occur between the molten steel and commonly used refractories in the steel foundry is of extreme importance to the quality of the final product. These interactions can be beneficial such as the use of magnesia refractories for additional control of sulfur or harmful in the case of chemical attack, erosive wear, and exogenous entrainment of inclusions. Monolithic refractories generally refer to all unshaped refractories that are installed as some form of suspension with a binder that hardens over time. Monolithic refractories are used extensively by steel foundries in gunning mixes, patching materials, as rammables, and as coatings. Without a proper binder system, monolithic refractory technology would be impossible. Binders are classified as hydraulic, chemical, organic, or ceramic (sintered). Chemical binders are inorganic, non-hydraulic, and obtain suitable green strength at room temperature. These chemical bonded refractories have widespread use in the steel foundry. The two chemically bonded monolithic refractories in the current study can be classified as phosphate bonded (90 RAM PC Plastic Monolithic refractory) and a silicate bonded (D11NP) alumina refractory. Phosphate bonded refractories are some of the most common chemical binders used in monolithic refractory patch and as capping material for ladles and induction furnaces. Some of the advantages of phosphate bonded refractories include a fast heat up with no need for curing, excellent repair properties because of good bonding between the phosphate bonded refractory and the fired ceramic substrate, resistance to CO attack, and excellent thermal shock properties. Phosphate bonded refractories contain phosphoric acid that reacts with metal hydrides or oxides to form salts that function as the bonding agent. The reaction occurs slowly at room temperature

and the product of the reaction is mono-aluminumphosphate, or MAP, $Al(H_2PO_4)_3$.

During heating, phosphate bonded refractories will gain strength as the MAP loses water.

The MAP will undergo several transformations during heating with final transformation

to P_2O_5 in the temperature range of 1300 to 1600°C. Phosphate binders in monolithic

refractories form an adherent MAP bond with fired high alumina ceramics, such as

crucibles used for induction melting. Figures 3.3 (a and b) show that in the current study,

the phosphate bonded refractory has better adhesion to the alumina crucible at high

temperature and less propensity for cracking than the silicate bonded refractory.

However, significant refractory-metal interaction was observed between the steel and the

phosphate bonded refractory and chemistry results showed phosphorus pickup in the re-

melted steel from 0.002%P to more than 0.14%P, as shown in Table 3.2. Phosphorus

pickup from phosphate bonded refractories has not previously been reported in high

manganese steels without aluminum such as Hadfield steels. However, phosphorus

reversion in liquid iron from the dissociation of P_2O_5 in the presence of aluminum

deoxidation is thermodynamically favorable and has been reported by several authors.[14-18] Therefore, the results of this study suggest that the high aluminum content in Fe-Mn-

Al-C steels is sufficient to react with the phosphate binder, forming corundum with

phosphorus reversion into the liquid steel. In a recent study by Suk et al.[14], experimental

and theoretical models showed reaction of P_2O_5 with aluminum to form P_4 gas at

steelmaking temperatures and then absorption of phosphorus into the melt according to

the following over-all reaction.[14-18]

$2P_2O_5 + 20/3Al \rightarrow 4P + 10/3\ Al_2O_3$ (1)
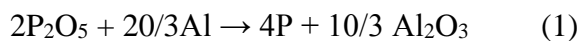
$\Delta GP = -3,161,800 + 81.91T$ J/mol

A plot of the free energy for P_2O_5 dissolution by aluminum and reversion of P into the liquid melt versus temperature is given in Figure 3.11. It is shown that the Gibbs free energy is strongly negative during steelmaking temperatures and this indicates that significant phosphorus pickup from phosphate bonded refractories during melting and melt handling is possible for steels containing large amounts of aluminum. The dissolution of P_2O_5 by aluminum is shown in equation 1 to create alumina (corundum) and a small amount of corundum was found at the interface between the phosphate bonded refractory and the surface of the solidified steel as shown in Figures 3.3(a) and 1.4. This phase was not noted in the steel that was melted against the silicate bonded refractory. Additionally, the steel melted against the phosphate bonded refractory showed a significant loss of aluminum, from 8.8 to 7.1%Al, and a gain in silicon, from 1.6 to 2.6%Si, as shown in Table 3.2. In comparison, the steel that was melted against the silicate bonded refractory is similar to the chemistry before re-melting, with only a slight increase in silicon. In the case of the steel melted against the phosphate bonded refractory, the decrease in aluminum content is likely due to the reduction of P_2O_5 and formation of Al_2O_3. The increase in silicon is likely from the reduction of silicates present in both refractories by aluminum in the melt. It is interesting to note that silicon was higher in the steel melted against the phosphate bonded refractory. Both steels also contained slightly higher carbon levels after re-melting. It is possible that using graphite during this experiment to scavenge remaining oxygen may have produced a reducing CO atmosphere, and this in addition to the high aluminum content of the melt, may have played a part in destabilizing the alumino-silicate refractories. Further studies are needed to determine these complex interactions. What is certain is that phosphorus pickup from

phosphate bonded refractories is significant in high manganese and aluminum steels and these refractories should be avoided during melting and melt handling.

Examination of the resulting microstructures provided an opportunity to observe the as-cast structures in high manganese and aluminum steel. Significant research has been presented with regard to microstructure/mechanical property relationships in the Fe-30Mn-9Al-(0.5-1.6)Si-0.9C-0.5Mo system, however most of these studies have reported on these alloys in the solution treated or solution treated and aged condition.[1,3,6-10,12,13] Studies of the as-cast structure have not been widely reported in high Mn and Al steels. In the current study, reversion of phosphorus into the steel during melting and solidification combined with slow cooling rates produced a highly segregated microstructure with large continuous areas of a eutectic phosphide phase in interdendritic areas and on grain boundaries as shown in Figures 3.6 (a) and 3.7 (c and d). EDS chemical analysis in Table 3.4 confirmed that this phase was rich in Mn, C, Si, Mo, and P when compared to the surrounding austenite matrix.
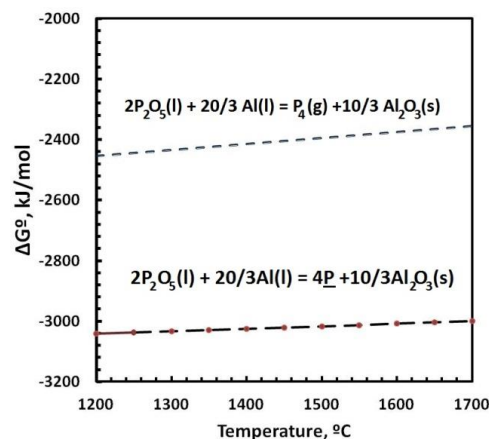
Figure 3.11: The Gibbs free energy for P2O5 dissolution by aluminum and reversion of P into the liquid melt shows that Gibbs free energy is strongly negative during steelmaking temperatures and this indicates that significant phosphorus pickup from phosphate bonded refractories during melting and melt handling is possible for steels containing large amounts of aluminum.

38

A similar phosphorus rich eutectic phase similar to steadite in cast iron has been previously reported by Howell et al.[10] in a solution treated Fe-30Mn-9Al-1Si-0.9C-0.5Mo steel with 0.07%P. The phosphide eutectic observed by Howell et al. was found in interdendritic areas and was identical in morphology to areas of the phosphide eutectic observed in the current study. This phosphorus containing eutectic was reported to be very hard and brittle with a hardness of 520 BHN (compared with austenite at 308 BHN) and was linked to low energy intergranular fracture and significant loss of room temperature notch toughness.[10] Regrettably, Howell et al. did not report in detail on the structure of the eutectic phosphide and they did not characterize the individual phases.[10] The phosphide eutectic in high Mn and Al steels has not been reported on in the as-cast condition, however, in solution treated steels (2 hrs at 1050°C) the phosphide eutectic has been reported in steels with as low as 0.018% P.[8] It is thus likely that in the as-cast condition, the critical amount of phosphorus to avoid this P-eutectic is much less and heavy segregation of phosphorus would magnify this effect. In as-cast and annealed Hadfield steels without aluminum, phosphorus has been reported to segregate in interdendritic regions and at grain boundaries and form binary eutectic phosphides consisting of austenite and iron phosphide that are similar to the morphologies observed in the current study.[19-22] Although phosphorus is particularly a problem in Hadfield steel with large section sizes, in section sizes less than 25mm phosphorus levels as high as 0.06%P can be tolerated without severely degrading high temperature plasticity.[19] D. Shulik et al. studied the influence of cooling rate and phosphorus contents in the range of 0.016-0.149% P on the formation of the phosphide eutectic in a (G13) Hadfield steel and found that the phosphide eutectic was found only in exceptional circumstances after slow

cooling when the phosphorus content was as low as 0.016%P.[21] The phosphorus eutectic

was not observed in 0.016%P castings that were quenched directly after solidification

from 1100°C. However, at all cooling rates, the as-cast microstructure of the higher

phosphorus specimens contained widespread areas of eutectic that was either globular

and in interdendritic areas or consisted of a thin film that coated grain boundaries.[21]

Insipient melting of the P-eutectic and wetting of austenite grain boundaries during

annealing has been reported by several authors and solution annealing temperatures are

recommended to be performed below 1100°C-1200°C.[19,21,22] In the current study, re-

melting of the low phosphorus steel against the phosphate bonded refractory resulted in

phosphorus pick-up from 0.002% to >0.14%P with as much as 10% of the phosphide

eutectic phase which was found both in interdendritic regions as well as to significantly

coat grain boundaries as shown in Figures 3.7 (c) and (d) and Figures 3.10 (a) and (c).

This is consistent with previous observations of the eutectic phosphide in Hadfield steels

with 0.07 to > 0.1%P were the as-cast steels contained both globular and grain boundary

eutectic films that can form during solidification or during annealing at too high of a

temperature.[22] The chemistry of the of the phosphide eutectic in the current study was

found to be rich in Mn, P, Mo, C, and Si as shown in Table 3.4. These results are similar

to the chemistry of the phosphide eutectic observed in a Hadfield steel by Kuyucak et

al.[22] which was also found to be rich in P, C, and Mn. As shown in Figure 3.10 (a),

lamellar κ-carbide was found along grain boundaries, often in combination with the

phosphorus eutectic. This is also consistent with previous research in as-cast Hadfield

manganese steels that show that eutectic carbide colonies can form along the trailing

edges of the phosphide eutectic.[20]

The coarse lamellar κ-carbide observed on the grain boundaries of the high phosphorus steel in the current study was not observed in the steel that was re-melted on the silicate bonded refractory and only areas of fine continuous grain boundary κ-carbide and homogenously precipitated matrix κ-carbide were observed as shown in Figures 3.7 (a) and (b) and Figure 3.8 (a). In addition, some areas of the lamellar κ-carbides in the high P steel were slightly rich in phosphorus. The major difference in the chemistries between the two steels in the current study is the amount of phosphorus and silicon. This suggests that the presence of phosphorus and also silicon stabilize κ-carbide in the as-cast condition and this is consistent with both experimental observations of age hardened steels with different amounts of phosphorus and silicon as well as first principles density functional theory calculations.[7,8,10,11] Silicon has been shown to increase the activity of carbon in solid solution austenite and stabilize carbide formation in both Hadfield steels as well as in high Mn and Al steels.[19,23] Phosphorus in high Mn and Al steels has been shown to accelerate age hardening and both matrix and grain boundary κ-carbide precipitation and first principles calculations show that phosphorus substitution in aluminum lattice positions within the κ-carbide is most thermodynamically favorable.[8,11,23]

In contrast to the high phosphorus steel, the micro-constituents in the as-solidified low phosphorus steel that was melted in contact with the silicate bonded refractory consisted mainly of an austenite matrix, continuous grain boundary κ-carbide, small isolated areas of ferrite and plate-like κ-carbide as shown in Figures 3.7 (a and b) and Figure 3.8 (a). This is consistent with previous reports by Chakrabarti et al. who reported on Fe-Mn-Al-C steels with 5.5 to 9.8% Al and 0.27 to 0.91%C.[24] The matrix was mainly

41

austenite, complex carbide, and differing amounts of ferrite.[24] Ferrite increased with increasing aluminum content and decreasing carbon. Some interdendritic regions and grain boundaries in the low P steel were also shown to have areas of alloy carbides that were determined by EDS analysis to be rich in Mn, Mo, C, and Si and this is consistent with M_3C type carbides that have previously been reported in Cr bearing Hadfield steel.[24]

Therefore, the results of the current study show that there is significant reaction between high manganese and aluminum steels and phosphate bonded refractories. Therefore these refractories should not be used during melting or melt handling of these steels.   Significant reaction between Fe-Mn-Al-C steel and the silicate bonded refractory was not observed and these refractories should be used in substitution for phosphate bonded monolithic refractories when melting high manganese and aluminum steels.

3.6 Conclusion

The interaction between two commercially available phosphate and silicate bonded alumina refractories and a high manganese and aluminum steel was studied during melting. Two revert samples of chemistry Fe-30Mn-9Al-1.6Si-0.9C-0.5Mo (0.002%P) were melted under protective atmosphere in a high purity alumina crucible lined with the phosphate and silicate bonded refractories, respectively. Melting in contact with the phosphate bonded refractory resulted in significant phosphorous pickup in the steel of more than 0.14 wt.%P. This is suggested to be the result of the reduction of the phosphate binder by the high aluminum present in these steels. The high phosphorus stabilized widespread formation of a brittle phosphorus rich eutectic phase that coated the majority of austenite grain boundaries. However, the steel melted in contact with the silicate bonded refractory showed little reaction with the refractory with a phosphorous content of 0.001 wt.%. The results of this study show that phosphate binders should not be used during the melting or melt handling of high manganese and aluminum steels as it can result in significant phosphorus pickup in the melt. The silicate bonded refractory showed little reaction with the steel and should be used as a substitute for phosphate bonded monolithic refractories.

3.7 References

1. G. Frommeyer and U. Brux, Microstructures and Mechanical Properties of High-Strength Fe-Mn-Al-C Light-Weight TRIPLEX Steels, *Steel Research Int*., Vol. 77, pp. 627-633 (2006).

2. Y. Sutou, N. Kamiya, R. Umino, I. Ohnuma, and K. Ishida, High-strength Fe-20Mn-Al-C Based Alloys with Low Density, *ISIJ International*, vol 50, pp. 893-899 (2010).

3. L. Bartlett, A. Dash ,D.C. Van Aken, V.L. Richards, and K.D. Peaslee, "Dynamic Fracture Toughness of High Strength Cast Steels," AFS Transactions, paper 12-054 (2012).

4. I. Kalashnikov, O, Acselrad, A. Shalkevich, L. Chumokova, and L. Pereira, Heat Treatment and Thermal Stability of FeMnAlC Alloys, *Journal of Materials Processing Technology*, vol 136, pp. 72-79 (2003).

5. Y. Kimura, K. Handa, K. Hayashi, and Y. Mishima, Microstructure and Ductility Improvement of the Two-phase γ-Fe/κ-(fe,Mn)$_3$AlC Alloys in the Fe-Mn-Al-C System, *Intermetallics*, vol 12, pp. 607-617 (2004).

6. R. Howell, T. Weerasooriya, and D. Van Aken, Tensile, High Strain Rate Compression and Microstructural Evaluation of Lightweight Age Hardenable Cast Fe-30Mn-9Al-XSi-0.9C-0.5Mo Steel, *Transactions of the American Foundry Society*, (2008).

7. L. Bartlett and D.C. Van Aken, "High Manganese and Aluminum Steels for the Military and Automotive Industry," JOM, Vol. 66, No. 1, p.1770 (2014).

8. L.N. Bartlett, R. Howell, D.C. Van Aken, and K.D. Peaslee, "Effect of Phosphorus and Silicon on the Precipitation of κ-carbides in Fe-30%Mn-9%Al-X%Si-0.9%C-0.5%Mo Alloys " Transactions of the American Foundry Society, Vol. 118, Paper No. 10-069, P 413-424, (2010).

9. R.A. Howell, J.M. Montgomery, and D.C. Van Aken: J. AIST, vol. 6. pp. 168-176 (2009).

10. R.A. Howell and D.C. Van Aken, "Microstructural and Fracture Behavior of Phosphorus Containing Fe-30Mn-9Al-1Si0.9C-0.5Mo Alloy Steel," Metallurgical and Materials Transactions A, Accepted 2015.

11. N.I. Medvedeva, R.A. Howell, D.C. Van Aken, and J.E. Medvedeva, Phys. Rev. B 81, 012105 (2010).

12. A. Schulte, S. Lekakh, D. Van Aken, and V. Richards, Phosphorus Mitigation in Cast Lightweight *Fe-Mn-Al-C* Steel, *114th Metalcasting Congress*, March 19-23, 2010, Orlando, FL.

13. L.N. Bartlett, D.C. Van Aken, S. Lekakh, and K.D. Peaslee, "Mechanical Properties of Cerium Treated Fe-Mn-Al-C Steel Castings," AFS Transactions, Vol. 119, pp. 545-560 (2011).

14. M. Suk, S. JO, S. Kim, K. Lee, and J. Park, "X-Ray Observation of Phosphorus Vaporization from steelmaking Slag and Suppression Method of Phosphorus Reversion in Liquid Iron," Metallurgical and Materials Transactions B, Vol. 37B, pp. 99-107 (2006).

15. J.F. Elliott, M. Gleiser, and V. Ramakrishna: Thermochemistry for Steelmaking, Addison-Wesley, London, vol. II, pp. 160-165, (1963).

16. E.T. Turkdogan and J. Pearson: J. Iron Steel Inst., pp. 398-401 (1953).

17. M. Yamamoto, K. Yamada, L.L. Meshkov, and E. Kato, Trans. Iron Steel Inst. Jpn., vol. 22, pp. 262-268, (1982).

18. E.T. Turkdogan, Physical Chemistry of High Temperature Technology, Academic Press, New York, NY, (1980).

19. C.S. Mahlami and X. Pan, "An Overview on High Manganese Steel Casting," Proceedings of the 71st World Foundry Congress, May 19-20 Bilbao, Spain (2014).

20. S. Kuyucak and R. Zavadil, "On the Heat-treatment of Hadfields Austenitic Manganese Steels Part VI: Impact toughness microstructure, macro and microsegregation in large wedge block castings," AFS Transactions, (2003).

21. D. Shulik, L. Kamarash, Y. Vilchko, and P. Dzugas, "Phosphide Eutectic in a Hadfield Steel Structure," Translated from Metallovedenie I Termicheskaya Obrabotka Metallov. No. 2, pp. 2-3 (1992).

22. S. Kuyucak and R. Zavadil, "On the Heat-treatment of Hadfields Austenitic Manganese Steels Part II: Metallographic Studies," AFS Transactions, pp. 21-55 (2000).

23. L. Bartlett, D. Van Aken, J. Medvedeva, D. Isheim, N. Medvedeva, and K. Song, "An Atom Probe Study of Kappa Carbide Precipitation and the Effect of Silicon Addition," Metallurgical and Materials Transactions A, Vol 45A, pp. 2421-2435 (2014).

24. Prodhan, A., Charkrabarti, A. K., "A Study on Cast Fe-Mn-Al-Si-C Alloys," AFS Transactions, vol. 37, pp. 35-46 (1990).

25. S. Kuyucak and R. Zavadil, "On the Heat-treatment of Hadfields Austenitic Manganese Steels Part VIII: Studies on Microcharacterization," AFS Transactions, pp. (2004).

4. EVALUATION OF STEEL-REFRACTORY INTERACTIONS DURING MELT TRANSFER OPERATIONS OF HIGH MANGANESE AND ALUMINUM STEELS

R. Rahman[1] and L.N. Bartlett[2]

[1]Texas State University, San Marcos, TX
[2]Missouri University of Science and Technology, Rolla, MO

.

4.1 Abstract

Austenitic high manganese and aluminum cast steels of nominal composition Fe-30%Mn-9%Al-1%Si-0.9%C-0.5%Mo have excellent combinations of strength and ductility and are almost 15% less dense than low alloy steels. However, the presence of phosphorus in levels greater than about 0.006 wt.% has a detrimental impact on ductility and toughness. Recent studies have shown that phosphorus pickup of greater than 0.14% is possible when these steels are melted in contact with commonly used phosphate bonded refractories. The current study evaluates steel-refractory interactions in a nominal composition Fe-30%Mn-9%Al-0.75%Si-0.9%C-0.5%Mo steel during ladling operations when there is much shorter residence time for the steel to be in contact with the refractory. Results showed that when the phosphate refractory was used to coat the ladles, this resulted in only a slight increase in phosphorus however, Si increased from 0.74 to 0.97% and carbon increased slightly from 1.06 to 1.13%. Age hardening was evaluated as a function of time at 530°C and the results show only a slight increase in hardening for the castings poured from phosphate bonded refractories. The room temperature breaking energy was evaluated for specimens in the solution treated and 10hr aged condition. The solution treated breaking energy was highest for the specimens poured from the phosphate bonded refractory ladles and this is attributed to an increased amount of carbon in solid solution. Ageing for 10hrs at 530°C sharply reduced the breaking energy from an average of 150 J to less than 5 J.

4.2 Introduction

Fully austenitic high manganese and aluminum steel castings typically contain 15-30 wt.% Mn, 3-12 wt.% Al, 0.3-1.2 wt.% C.[1-5] Manganese and carbon stabilize a fully austenitic microstructure when solution treated above 950°C and aluminum lowers the overall density by up to almost 15% in a Fe-30wt.%Mn-9 wt.% Al-0.9wt.%C-0.5wt.%Mo Steel.[2] It should be noted that all compositions given in the following text are expressed as weight percent unless otherwise stated. High manganese and aluminum steels that contain greater than about 6%Al and 0.6% C are age hardenable via the homogenous precipitation of nanometer sized κ-carbide within the matrix austenite for aging temperatures in the range of 400-700°C.[6-13] Mechanical properties of these alloys are thus a function of both chemical composition and the degree of age hardening. Much recent research has centered around variations of the Fe-30%Mn-9%Al-(0.5-1.6%)Si-0.9%C-0.5%Mo steel which is being considered as a lightweight alternative to quenched and tempered Cr and Mo steel in high energy absorbing applications such as for the military and automotive industries.[2,5] Bartlett et al. compared the dynamic fracture toughness of low phosphorus (<0.003%P) Fe-30%Mn-9%Al-0.5%Si-0.9%C-0.5%Mo steel in the solution treated and aged (at 530°C) conditions with the toughness of a commercially cast, quenched and tempered, SAE 4130 steel.[5] When compared with the 4130 steel, they found an increase from 135 to 715 kJ/m^2 in dynamic toughness for the Fe-Mn-Al-C steel in the as-solution treated condition.[5] Age hardening and the precipitation of κ-carbide sharply reduces toughness and transitions the fracture mode from ductile to a cleavage-like fracture that may be intergranular or transgranular in nature.[14] However, when impurity levels of phosphorus are low, typically 0.006%P or

lower, toughness and strength combinations can exceed that of quenched and tempered 4130 steels.[5]

It has been shown that phosphorus adversely affects the mechanical properties of high manganese and aluminum steels and this is especially true of toughness and elongation.[2,5,15] In the solution treated condition, an increase in the phosphorus content from 0.001%P to 0.07%P decreased the Charpy V Notch (CVN) impact energy from 200 to 28J for a Fe-30Mn-9Al-1Si-0.9C-0.5Mo nominal composition steel.[5] Phosphorus has been shown to increase the kinetics of κ-carbide precipitation in high Mn and Al steels and this results in a profound loss of toughness.[5] According to a study by Howell et al. of an Fe-30Mn-9Al-1Si-0.9C-0.5Mo steel aged hardened for 10hrs at 530°C, increasing phosphorus levels from 0.001% to 0.07% P resulted in up to 94% reduction in CVN toughness from 138 J/cm^2 to 2 J/cm^2.[15] Medvedeva et al. have predicted using first principles calculations that when phosphorus is present, it preferentially substitutes for aluminum positions in the κ-carbide structure and this creates open volume defect along the $<100>_k$ resulting reduction in the cleavage stress of κ-carbide by 45%.[28] Furthermore, phosphorus segregation to grain boundaries has been shown to promote precipitation and growth of k-carbide on the grain boundaries causing a decrease in toughness.[15] It has been shown that rare earth additions after calcium treatment can reduce the amount of phosphorus in solution, however, this results in the formation of heavy rare earth oxides, sulfides, and phosphides that do not float during stirring and sharply reduce toughness.[17,] Therefore phosphorus levels should be kept as low as possible, less than 0.01-0.006%P, and therefore foundries should use high purity charge materials during induction melting. Interestingly, and even when pure charge materials

have been utilized, higher than expected amounts of phosphorous, up to 0.01% P, have been routinely reported as well as hard to control silicon levels.   As the potential source of unwanted phosphorus in the melt, furnace and ladle refractories was proposed but never confirmed by Howell et al.[18]

Monolithic refractories have widespread applications in steel foundries for better structural integrity, a continuous body without any joints, and ease of installation.[19] Non-hydraulic, inorganic chemicals like phosphoric acid, phosphates, and silicates are used in different type of monolithic refractories as a binding agent. These binders help the refractories to harden over time at room temperature and maintain a strong bond at elevated temperatures.[19] At steel making temperature refractories are subject to wear and chemical attack by the molten steel and reaction can occur between the molten steel and refractory linings can result in entrainment of course nonmetallic inclusions as well as impurity elements into the melt. Phosphate bonded refractories commonly termed Plastic Rammables are commonly used by iron and steel foundries to set the crucible in the induction furnace, line the perimeter of the furnace and ladle as well as a patch material. A recent study conducted by the authors on a low phosphorus (<0.002%P) Fe-30Mn-9Al-1Si-0.5Mo steel re-melted for extended time in contact with a commonly used phosphate bonded plastic refractory showed manganese and aluminum steels picked up more than 0.14% phosphorus when in contact for a prolonged period.[20] In addition, an increase in C and Si content in the steel was also noted. The current study evaluates the steel-refractory interactions that may result between two commonly used refractories (phosphate bonded and silicate bonded) during ladling and melt handling operations.

4.3 Experimental Procedure

High manganese and aluminum (Fe-Mn-Al-C) alloy steels under investigation were produced in induction furnace with 86 lbs. capacity pure alumina made crucible per batch in protective argon atmosphere at continuous flow of 60 SCFH. During the melting process, high purity charge materials such as graphite, electrolytic manganese, ferro-molybdenum, and ferro-silicon were used to obtain steels with target chemistry of 30% Mn-9% Al-1% C-1% Si and phosphorus level below 0.006% while covering the furnace with "refractory ceramic fiber blanket". Temperature of the furnace was continuously monitored and recorded using thermocouples throughout the melting process. Tapping of the melt into fire heated transfer ladles coated with refractories materials were done at 2868°F (1575°C).

Long before the actual pour two individual alumina made transfer ladles with holding capacity of 9.5 kg of melt were prepared by coating those with two different monolithic refractories such as phosphate bonded plastic rammable 90 RAM PC (90.5% Al_2O_3, 4.9% SiO_2, 3.6% P_2O_5, 0.4% ($Na_2O + K_2O$), 0.2% Fe_2O_3, 0.1% CaO, 0.1% MgO, 0.2% other) and castable silicate bonded D11NP (figure 4.1: b) (90% Al_2O_3, 10% Na_2SiO_3). The 90 RAM PC refractory was pounded and rammed on the inner surface of one ladle as shown in figure 4.1 (a). On the other hand, thick paste of D11NP refractory materials was prepared by mixing water prior to coating the inner surface of the 2nd transfer ladle (figure 4.1: b) and capping the induction furnace as seen in figure 4.1 (c). Refractory materials applied on ladles and furnace were air dried for 2 weeks prior to pour. Molten Fe-Mn-Al-C steels prepared in one heat were poured into 2 argon gas filled no-bake sand made modified charpy Y-block (figure 4.1: d) made of no-bake sand molds

from each individual refractory lined transfer ladle. Afterward charpy Y-block molds filled with melt were left under normal atmosphere to solidify completely. Cutting of gate system, riser section, charpy sections for milling, chemistry samples and sections for metallographic specimens from all the 4 charpy Y blocks were done by using water cooled abrasive saw.
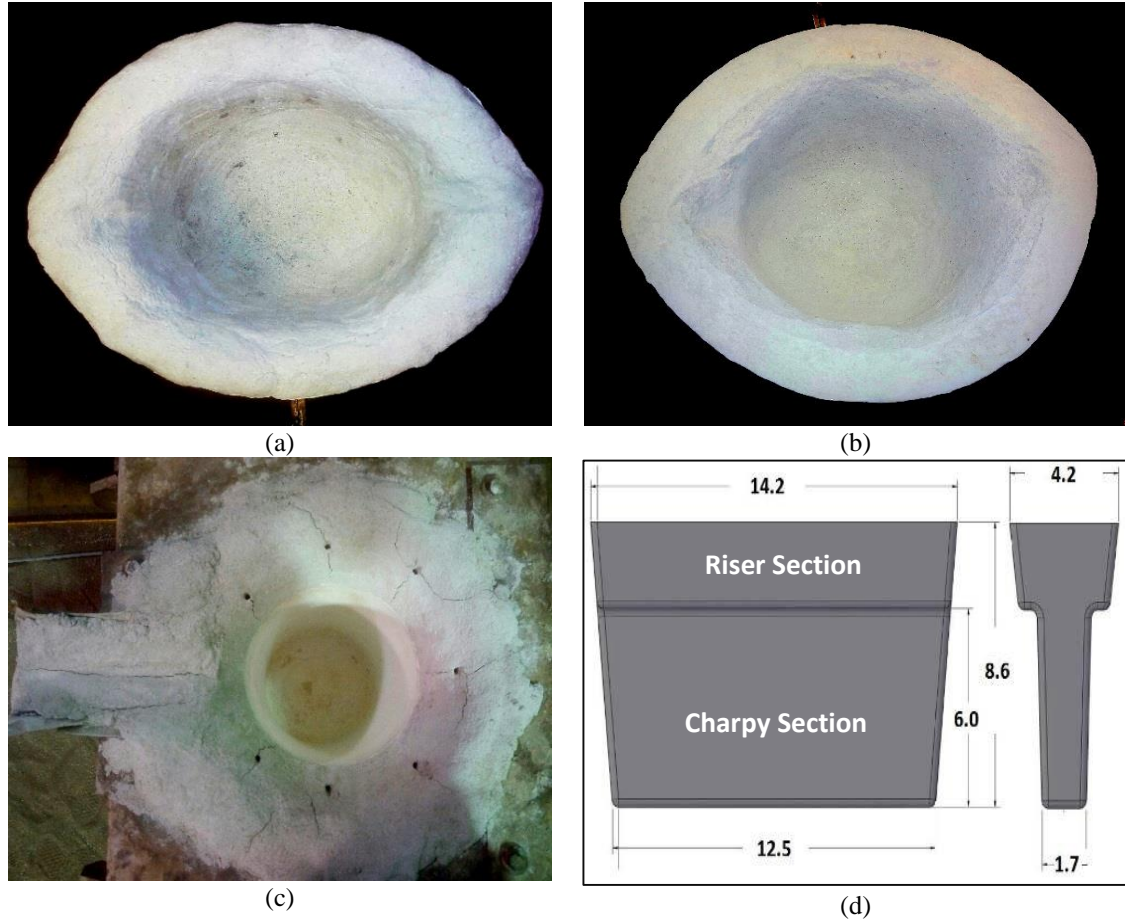
Figure 4.1: Transfer ladles made of alumina coated with (a) phosphate bonded monolithic refractory (b) silicate bonded monolithic refractory (c) induction furnace capped with silicate bonded monolithic refractory (d) modified charpy Y-block of steels prepared by pouring molten metal from refractory coated ladles into no-back sand molds.

The chemical compositions of the steel sample from 4 charpy Y-blocks were done by inductively coupled plasma (ICP) analysis. Riser section and charpy sections were solution treated at 1050°C for 2 hours on alumina ceramic tray containing pure graphite in high temperature box furnace and quenched in water. Afterwards each solution treated riser

53

section was cut into 10 pieces with dimension of (8±2)mmx42mmx26mm for the purpose of aging to understand the hardening behavior in relation to aging duration. Aging of the riser cuts was done at 530°C for different duration of 1, 3, 5, 10, 20, 30, 60, 100 hours in salt bath furnace followed by water quenching. Hardness measurements of the riser cuts were recorded both in solution treated and aged condition using Mitutoyo Rockwell Hardness Testing Machine (model: HR-500). The solution treated charpy sections were milled into ASTM E23 standard dimension of 55mm x 10mm x 10 mm charpy bars. Afterwards some of milled charpy bars obtained from each Y-blocks were aged at 530°C temperature for 10 hours in salt bath furnace followed by water quenching.

Measurement of hardness of each charpy bars blocks were taken on the bar surface. A "V" notch of each bar was broached using hand operated charpy notch broaching machine according to ASTM E23 standards for measuring CVN impact toughness using charpy impact tester. Charpy impact testing machine was used to measure impact energy. Afterward facture surface from broken charpy bars and sample made from below fracture surface for metallography were prepared using water cooled abrasive saw. Hardness of the charpy bars were again measured and recorded from the cross section of each broken charpy pieces. Refractory samples and steel scales samples for SEM analysis were prepared from both the transfer ladles. Nikon Epiphot 300 optical microscope was used for evaluating surface microstructure by applying standard metallographic techniques after mounting in Bakelite by heat-compression technique and polishing the as-cast, solution treated and aged metallographic specimens both in etched and un-etched condition where 5% Nital was utilized as etchant. FEI field emission scanning electron microscope (SEM) equipped with energy dispersive X-ray

spectroscopy (EDS) was used for the purpose of dimension measurement and analysis of

different microstructures' chemical composition.

4.4 Results

4.4.1 Optical inspection and chemical analysis

After the ladling trials were complete, the remaining steel was allowed to solidify

on the surface of each ladle. The ladles were allowed to air cool to room temperature and

the solidified steel skulls were removed from each refractory lined ladle as shown in

Figure 4.2 (a-d).   As shown in Figure 4.2 (c and d), the silicate bonded refractory coated

ladle shows no distinguishable color change of the refractory and very little evidence of

chemical or physical attack by the steel. The steel came away easily from the silicate

bonded refractory in one solid unit. However, color of phosphate bonded refractory

lining of ladle changed significantly from white to deep orange and brown as it appears in

Figure 4.2(a). The solidified steel skull shown in figure 4.2 (b) was not easily removed

from the phosphate refractory and this indicates the steel tended to wet the surface of the

refractory that may have led to significant chemical reaction during the holding time and

pouring into molds.

When referring to the experimental test castings, the following nomenclature will

be adopted. The first casting poured on the unused phosphate refractory ladle will be

denoted as Phos-1. The subsequent castings poured from the then used phosphate

refractory ladle will be denoted as Phos-2. The first casting poured on the unused silicate

refractory ladle will be denoted as Silicate-1. The subsequent castings poured from the

then used silicate refractory ladle will be denoted as Silicate-2. The chemical composition

of castings poured from each refractory coated hand ladle are shown in Table 4.1. The

expected composition of the steel is given for comparison. It should be noted that the

amount of phosphorus in this heat was expected to be 0.007%P and this is based mainly

on the higher than expected amount of phosphorus in the induction iron of 0.01%P. The phosphorus levels were similar between castings and varied between 0.006 and 0.01%P. This shows that there is not significant pickup of phosphorus during the rather short residence time between transferring to the hand ladle and pouring of the castings. It is interesting to note that the phosphorus level decreases from 0.01 to 0.006%P once the phosphate bonded refractory has been used. According to the chemistry data in table 4.1 all the samples other than Silicate-2 had higher C than target chemistry. It is to be noted that both in Phos-1 and Phos-2 contained higher Si content of roughly ~0.96% whereas both Silicate-1 and 2 had only around 0.74%. Other alloying elements as well as trace elements like Ni, Ti, Nb were similar in all the samples as shown in Table 4.1.

(a)   (b)

(c)   (d)
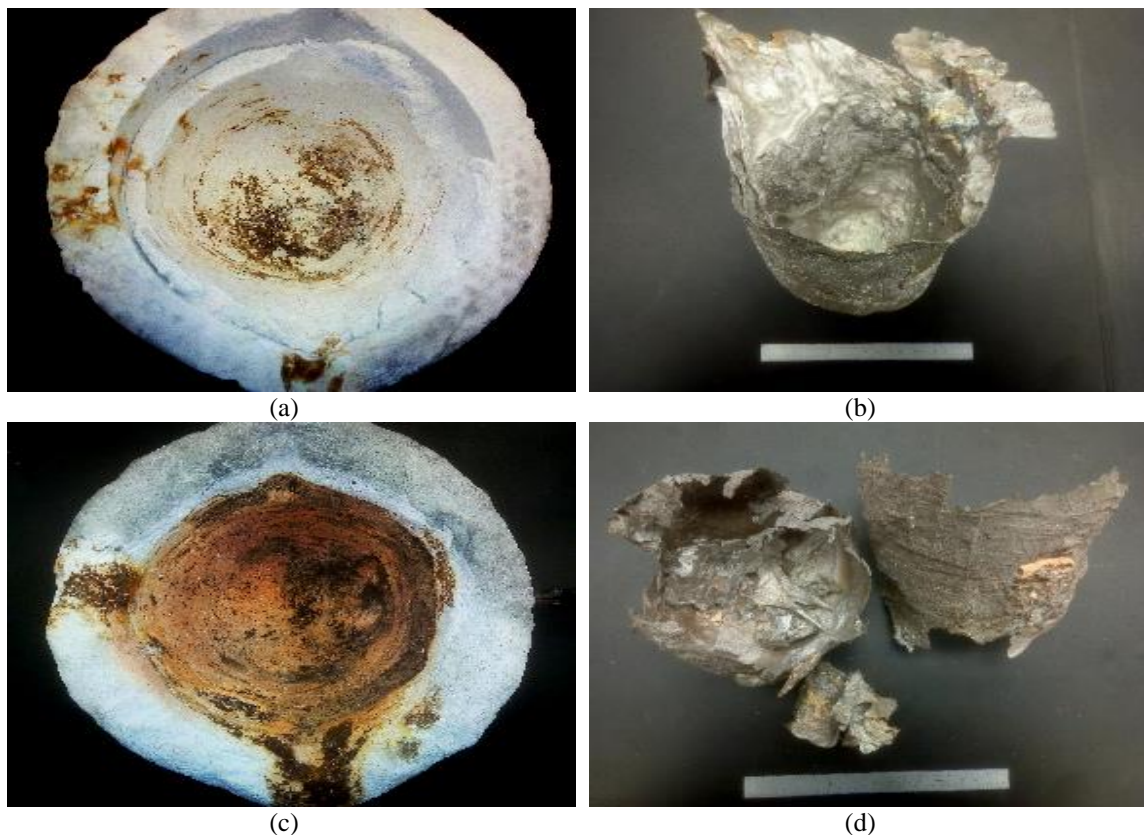
Figure 4.2: Transfer ladles after removal of the solidified skull of metal. (a) Phosphate bonded refractory and (b) corresponding skull. (c) Silicate bonded refractory and (d) corresponding solidified skull. (a and b)The metal adhered to the phosphate bonded refractory and was difficult to remove after solidification showing chips of entrained refractory in the solidified steel. (c and d) The steel showed little wetting of the surrounding

refractory and was easy to remove. The silicate refractory proved to be brittle and was easily chipped away after use.

Table 4.1: Target and actual chemistries of castings in weight percent.

Specimens	Sample Name	Fe	Mn	Al	Si	C	Mo	P	Ni	Ti	Nb
Target Chemistry		Bal.	30	9.3	1	1	0.50	<0.004			
Y block 1	Phos-1	Bal.	29.13	8.93	0.97	1.13	0.43	0.01	0.02	0.02	<0.01
Y block 2	Phos-2	Bal.	29.44	8.84	0.93	1.12	0.43	0.006	0.02	0.02	<0.01
Y block 3	Silicate -1	Bal.	29.28	8.89	0.74	1.06	0.43	0.007	0.02	0.02	<0.01
Y block 4	Silicate-2	Bal.	29.30	8.83	0.75	0.88	0.44	0.009	0.02	0.02	<0.01

4.4.2 Microstructural analysis

Specimens in the as-cast, solution treated, and aged conditions were sectioned from Y-block castings for microstructural analysis. The specimens were polished and etched with 10% Nital for about the same amount of time, 2-3 seconds. The optical micrographs of the as-cast microstructures from the respective castings are shown in Figures 4.3. The deep etching is the result of coarse κ-carbide precipitation in the matrix and on grain boundaries. Image analysis reveals that the Phos-1 specimen contained (figure 4.3: a) nearly 3 vol.% ferrite. Only a fraction of a percent of ferrite was observed in both as cast Silicate-1 and 2 castings as shown in Figure 4.3 (b) and (d) respectively. It is interesting to note that the ferrite in all of the as-cast samples appeared to have carbide or an intermetallic compound that has precipitated mainly near the ferrite-austenite interface.   This phase has not been previously documented in literature. Heavy grain boundary precipitation that is most likely κ-carbide was noted in all as-cast specimens as shown in Figure 4.3 (d). In addition, a small amount of a low melting point eutectic phase was noted some areas, Figure 4.3 (d).

After solution treating for 2 hours at 1050°C followed by water quenching there was a drastic reduction in the amount of ferrite that was observed for all samples as shown in Figure 4.4 (a and b).

(a)   (b)
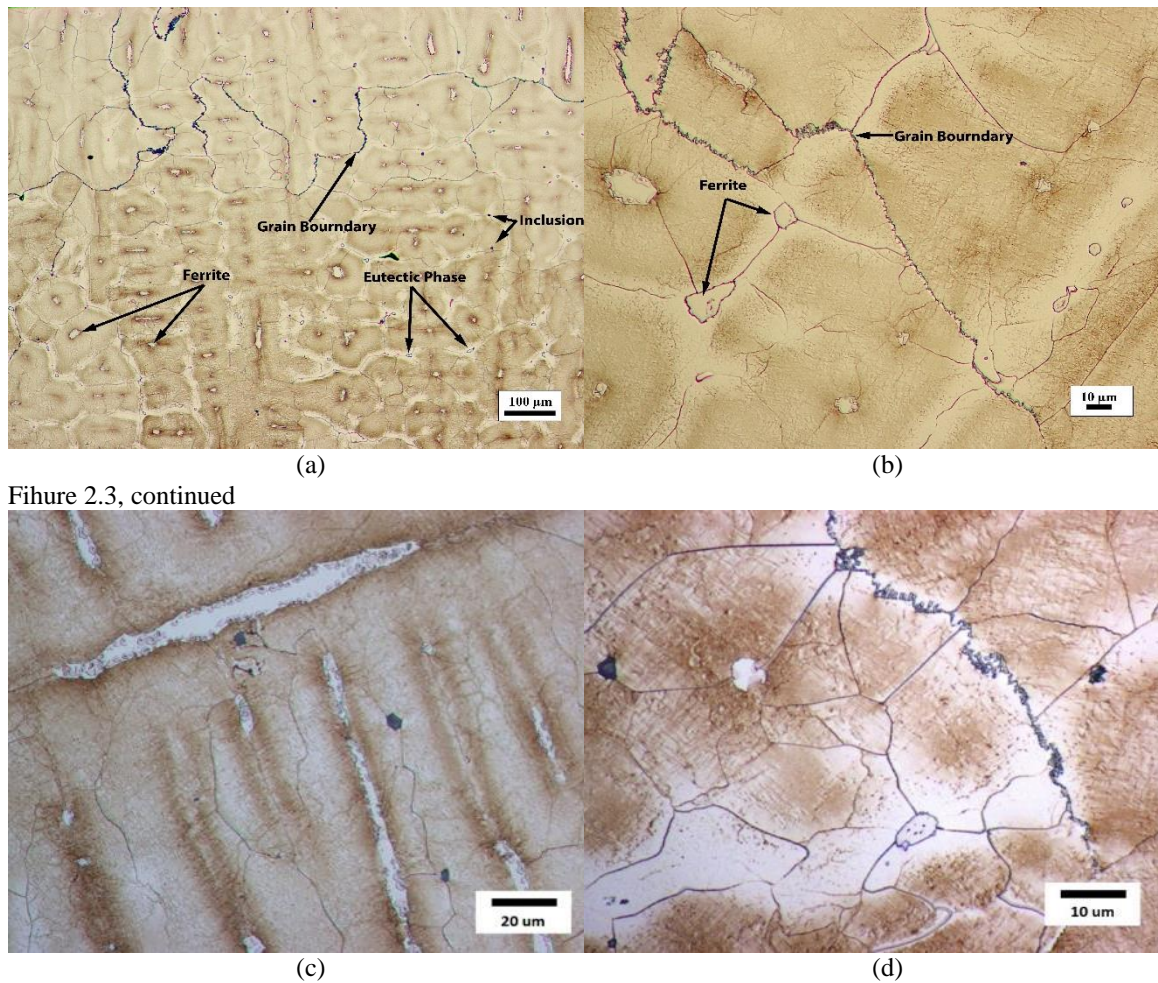
Fihure 2.3, continued

(c)   (d)

Figure 4.3: Optical micrographs of specimens in the as-cast condition were sectioned from the Phos. 1 (a and c) and Silicate 1 (b and d) castings. Deep etching is the result of matrix and coarse grain boundary κ-carbide precipitation. Primary skeletal ferrite is shown in the central regions of dendrite cores and secondary arms in all as-cast specimens but was most prevalent in castings poured from phosphate refractory coated ladles as shown in (a) and (c). Small amounts of a eutectic phase most consistent with steadite was found in interdendritic areas as shown in (d).

Upon solution treatment the carbide or intermetallic phase that was found to precipitate in the ferrite regions in the as-cast state   dissolved back into the matrix as shown in Figure 4.4 (c). The amount of grain boundary carbide has also significantly been reduced, but not completely eliminated in some areas as shown in Figure 4.4 (a and b). Additionally, the low melting point eutectic phase was completely eliminated after solution treatment in all castings as shown in Figure 4.4 (a and b). The microstructures optically observed in the solution treated condition were therefore quite similar between

the respective castings. The only major difference was a small amount of increased

retained ferrite content in the castings poured using the phosphate bonded refractories.

Figure 4.4 (c and d) shows the microstructure of the Phos. 1 and Silicate 1 castings,

respectively, after solution treatment and aging for 100 hours at 530°C. Widespread

continuous grain boundary precipitation is observed for both castings as well as some

course matrix precipitation that has become highlighted by the nital etch. With the

exception of retained ferrite content, the optical microstructures after aging were similar

between the different castings regardless of chemistry, as shown in Figure 4.4 (c and d).

(a)   (b)

(c)   (d)
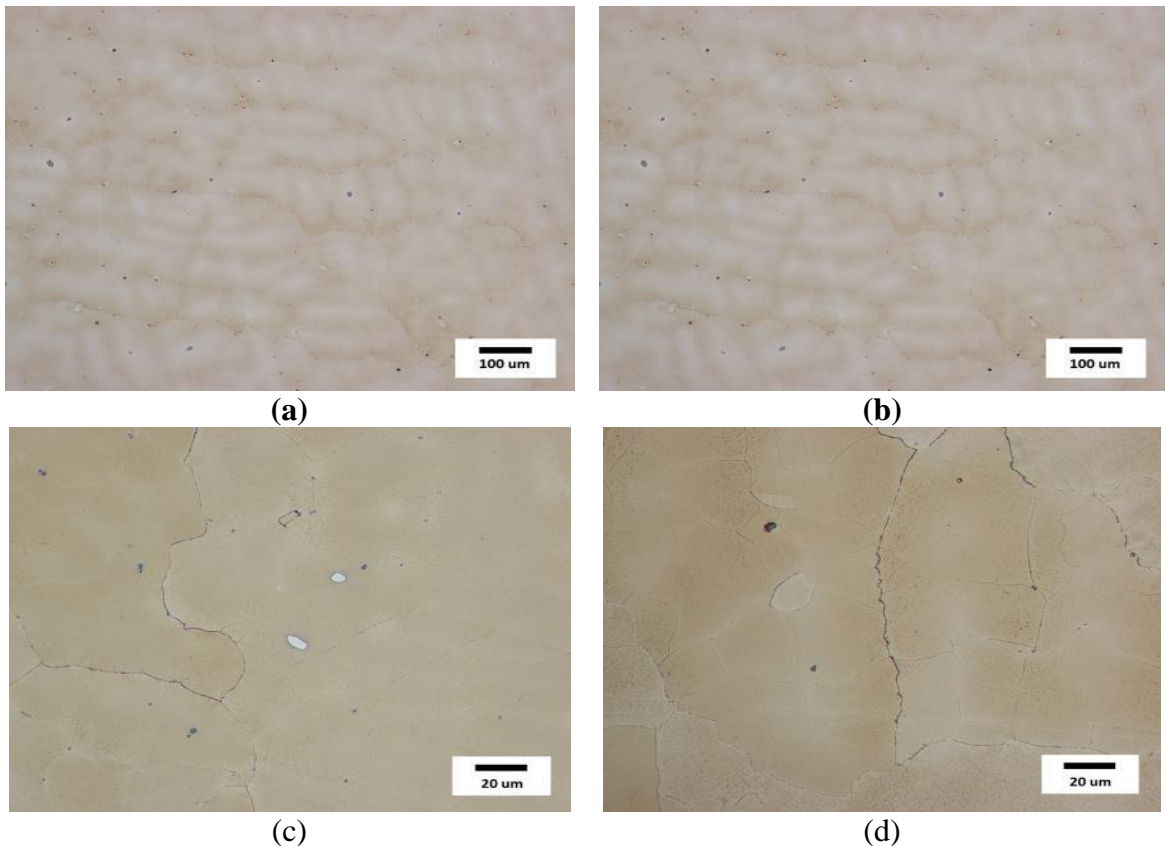
Figure 4.4: Optical micrographs of casting microstructures in the as-solution treated and quenched condition (a and b) and after aging for 100 hrs at 530°C (c and d). Much of the ferrite, grain boundary, and matrix precipitation have been eliminated after solution treatment at 1050°C and the Phos. 1 (a) and Silicate 1 (b) castings show a microstructure of nearly 100% austenite with some isolated areas of remaining grain boundary precipitation. The microstructures of the Phos. 1 and Silicate 1 castings are shown in (c) and (d) respectively, after aging for 100hrs. (c and d) Continuous precipitation on grain boundaries was widespread in both aged specimens. (c) After solution treatment the remaining ferrite (white contrast phase) was free of the second phase precipitation that was noted in as-cast specimens and this phase did not return with aging up to 100hrs at 530°C.

4.4.3 EDS analysis of microstructures

The identity of the different phases can be more accurately determined by using scanning electron microscopy, SEM, with energy dispersive X-ray spectroscopy, EDS. Figure 4.5 represents images of microstructures in as-cast sample obtained by using SEM. The corresponding chemistries of different phases were measured by EDS analysis and are provided in Table 4.2. Figure 4.5(a and b) shows the as-cast microstructure of the Phos. 1 and Silicate 1 castings, respectively. Primary ferrite is shown at the center of austenite dendrites. Interdendritic regions and grain boundaries contained a high amount of both continuous and cellular κ-carbide precipitation as shown in Figure 4.5 (a-c). Figure 4.5 (c) shows the microstructure of the as-cast Silicate 1 casting. Figure 4.5(c) shows cellular κ-carbide the interdendritic areas as well as mixed alloy carbides that are rich in Ti, Mo, and Nb. Alloy carbides were easily recognizable due to high z-contrast and angular shape. These carbides were not as prevalent as the κ-carbide phase which was found to heavily coat austenite grain boundaries as well as to precipitate in the matrix austenite as shown in Figures 4.5 (c and d). κ-carbide precipitation on grain boundaries and in the matrix tended to be greater and larger in the castings that were poured from the phosphate bonded refractory coated ladles as shown in Figure 4.5 (f).

The low melting point eutectic phase that was observed in the optical images was determined by EDS analysis to be rich in Si, P, C, and Mo as shown in Figure 4.5(d) and Table 4.2. This phase was noted to a certain degree in all castings and is most consistent with a form of steadite commonly encountered in manganese steels. A high magnification image of skeletal ferrite from the Silicate-1 casting is shown in Figure 4.5 (e) surrounded by dense matrix k-carbide precipitation, which is common in all as-cast

61

samples. K-carbide is shown to precipitate at the austenite-ferrite interface as shown in Figure 4.5(e). It is also interesting to note that the ferrite appears to be modulated in nature and this may be the result of further decomposition or ordering within the ferrite.

Solution treatment for 2hrs at 1050°C followed by a water quench dissolved almost all matrix and grain boundary carbide precipitation. Solution treated microstructures were similar between respective castings. A representative example of the solution treated microstructure is shown in Figure 4.6 (a) for the Phos. 2 casting. The solution treated microstructure shows little trace of grain boundary or matrix carbide precipitation. After aging for 100 hours at 530°C, homogenous matrix precipitation of cuboidal κ-carbide was noted to precipitate and coarsen along austenite <100> directions as shown in Figure 4.6 (b). The size of the κ-carbide was similar between castings, around 23-29 nm and tended to be larger in the castings poured from the phosphate bonded refractories. Grain boundary mixed alloy carbides and κ-carbides were also noted in some areas but this did not seen to depend on overall casting composition.

Table 4.2: EDS chemistries of different microstructural phase observed in as-cast microstructures of castings

Phase	Sample	C	Mn	Al	Si	Mo	P	S	Zr	Ti	Nb
Austenite	All	2-3	30-32	7.7-8.5	0.9	0.4	-				
Ferrite	All	-	20	10	0.6	-					
Phosphide Eutectic	All	0-5	44	3-5	2-5	-	1-2	0-2			
GB k-carbide	All	2-6	24-33	7-8.5	0.3-1.2	0-0.7					
k-carbide in ferrite	All	5	29	12	-	-					
Mixed alloy carbide	All	14-15	9-12	1.7-2.4	-	25-28			0-1	23-31	4-5
Matrix K-carbide	Phos-1	3.3	26	9.1	0.3						
	Silicate-1	3.7	26	9.0	0.5						
	Phos-2	3.3	27	9.2	0.4						
	Silicate-2	3.4	26	8.5	0.3						
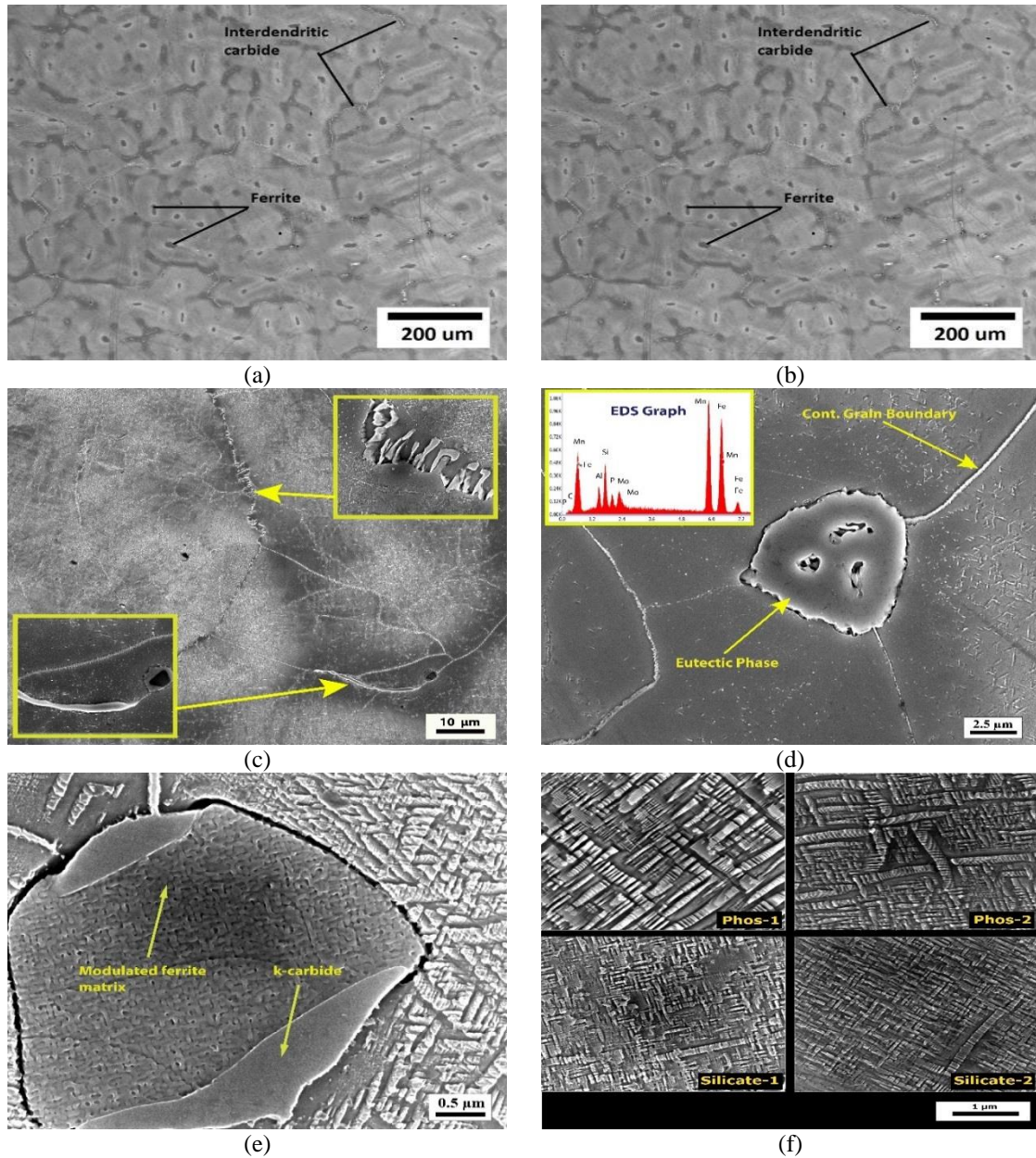
Figure 4.5: Secondary electron images of casting microstructures in the as-cast condition. (a) The Phos. 1 and (b) Silicate 1 castings show primary ferrite at the center of austenite dendrites and κ-carbide precipitation along grain boundaries and in interdendritic areas. (c) Continuous and cellular κ-carbide (top inset) precipitation was noted in interdendritic areas and along grain boundaries as well as varying amounts of a mixed Ti-Mo-Nb carbide (bottom inset) in the Phos. 1 casting as well as other castings. (d) The low melting point eutectic phase was found to a small extent in all castings and was located in interdendritic regions and was rich in Si, P, C and Mo. (e) Examination of the ferrite showed a modulated microstructure that may be evidence of some decomposition or ordering reaction. K-carbide precipitates at the ferrite-austenite interface during cooling. (f) Course matrix precipitation of κ-carbide was noted in all specimens but was most prevalent and much larger in size in the castings poured from the phosphate bonded refractories.

(a)	(b)

Figure 4.6: Secondary electron micrographs of the solution treated and water quenched Phos. 2 (a) and solution treated, water quenched, and aged 100hrs at 530°C condition. (a) In the solution treated condit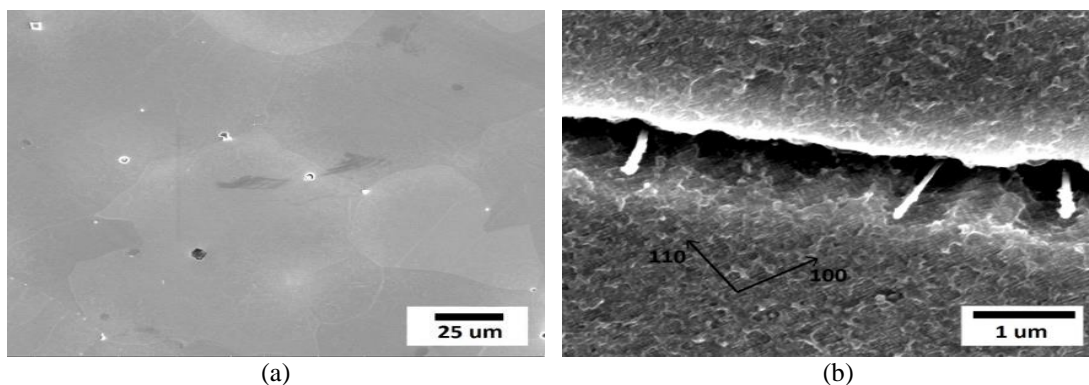ion, grain boundary and matrix κ-carbide are not observed. (b) After aging for 100 hrs, cuboidal κ-carbide that is about 20-30 nm in size has precipitated along austenite <100> is observed in the matrix and grain boundaries contain varying degrees of carbide precipitation.

4.4.4 Mechanical Properties

Rectangular specimens approximately 0.5" thick were solution treated for two hours at 1050°C, water quenched, and age hardened for up to 100 hrs at 530°C. Hardness measurements were taken from each specimen using the the Rockwell B and C scales and subsequently converted to an appropriate Brinell hardness number, BHN. Figure 4.7 shows the age hardening curves for the Phos. 1 and Silicate 1 castings (Figure 4.7 (a)) and Phos. 2 and Silicate 2 castings (Figure 4.7 (b)). Solution treated hardness is denoted at a time of 0.1 hrs and appears to be largely independent of chemistry. The Phos. 1 casting shows the highest hardening rate as shown in Figure 4.7 (a). After the phosphate bonded ladle is used to pour the first casting, the age hardening behavior of the Phos. 2 casting appears to be identical to that of the Sillicate 2 castings. Phos-1 and Silicate-1 both showed highest hardness of 395±6 BHN and 390±5 BHN, respectively, after 100 hrs of aging time. Interestingly, after 60 hours of aging both Silicate-2 and Phos-2 gained pick hardness of 374±7 BHN and 371±10 BHN, respectively. A comparison of the room temperature Charpy v-notch impact energies of the different castings in the as-solution treated and quenched condition and with a subsequent 10 hrs of aging at 530°C are

shown in Figure 4.8 (a). The corresponding and average hardness measurements are
shown in Figure 4.8 (b) and were taken from the charpy cross-sectional area. Figure 4.8
(a) shows that ageing 10 hours caused drastic reduction in CVN impact toughness of
between 94 and 97% in comparison to the corresponding solution treated charpy bars.

This effect seemed to be independent of the choice of refractory used to line the
pouring ladle with breaking energies for specimens aged 10 hrs ranging from 4-5 J. In
the solution treated condition, breaking energies were much higher and ranged from 96 J
for the Silicate 2 casting to 160 J for the Phos. 2 casting in the solution treated condition.
In general, the castings poured from the ladle lined with the phosphate bonded refractory
were observed to have a higher average breaking energy. Figure 4.8 (b) shows the
average hardness of the solution treated and aged Charpy test specimens. The solution
treated hardness was similar between the different specimens and varied between 203
BHN and 220 BHN. Hardness was similar in aged Charpy bars and varied between 365
and 370 BHN regardless of the choice of refractory used to coat the transfer ladle.
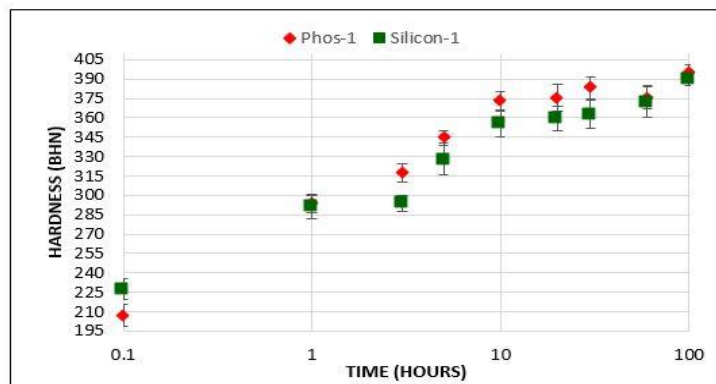
(a)

Figure 4.7: Age hardening curves for specimens solution treated at 1050°C, water quenched, and aged for
530°C for up to 100 hrs. The time of 0.1 hrs corresponds to the as-solution treated and quenched condition.
(a) The age hardening behavior of the Phos. 1 casting shows slightly higher age hardening kinetics when
compared to the Silicate 1casting. (b) After the ladles had been used to pour the first castings, it appears
that the age hardening behavior is nearly identical in the Phos. 2 and Silicate 2 castings
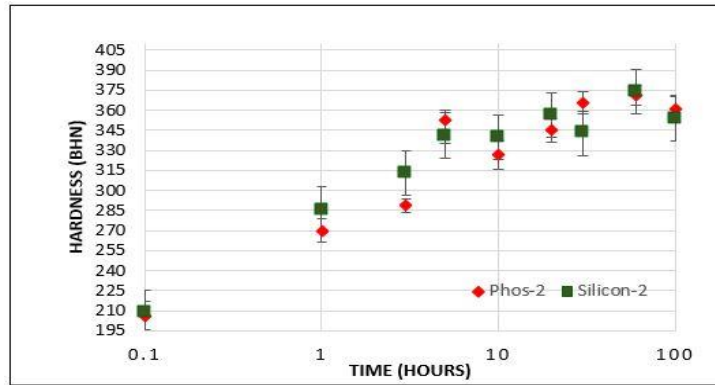
(b)

Figure 4.7: continued

Figure 4.7: Age hardening curves for specimens solution treated at 1050°C, water quenched, and aged for 530°C for up to 100 hrs. The time of 0.1 hrs corresponds to the as-solution treated and quenched condition. (a) The age hardening behavior of the Phos. 1 casting shows slightly higher age hardening kinetics when compared to the Silicate 1casting. (b) After the ladles had been used to pour the first castings, it appears that the age hardening behavior is nearly identical in the Phos. 2 and Silicate 2 castings
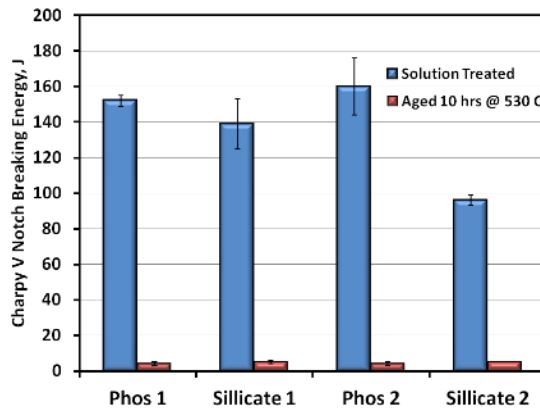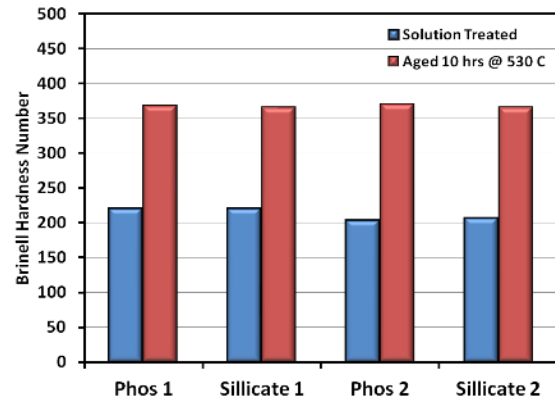
(a)   (b)

Figure 4.8: (a) Average room temperature breaking energy as a function of heat treatment shows that solution treated castings poured from the phosphate bonded refractory lined ladles generally had much higher breaking energies. Toughness dramatically decreases after aging for only 10 hrs at 530°C by 94 to 97% and seems to be independent of the choice of pouring ladle. (b) The solution treated and aged hardness values of Charpy specimens were independent of the choice of refractory used to coat the pouring ladle.

4.4.5 Fractography

Analysis of the fracture surface of selected test specimens was conducted utilizing the SEM. Figure 4.9 (a) and (b) shows the fracture surfaces of test bars in the solution treated condition for the Phos. 2 and Silicate 2 castings, respectively. The Phos. 2 casting had the highest breaking energy and is shown to have a completely ductile fracture surface in Figure 4.8 (a).

(c)   (d)

Figure 4.9: The fracture surfaces of representative Charpy test bars tested at room temperature and in the solution treated condition. (a) The fracture surface from th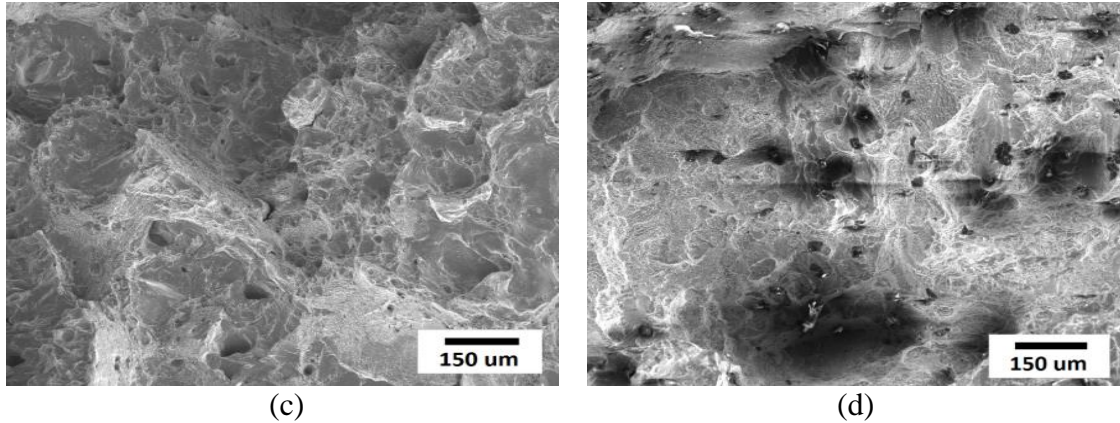e Phos. 2 casting shows a completely ductile fracture mode via microvoid nucleation and coalescence around inclusions and second phase particles. (b) The solution treated Charpy specimen from the Silicate 2 casting shows mainly ductile fracture with areas of low energy intergranular fracture. Large populations of inclusions and also bi-film defects were noted on the surface of test specimens.

The fracture surface from the solution treated Charpy bar from the Silicate 2 casting is shown in Figure 4.9 (b) to be mainly ductile in nature but also with areas of low energy intendendritic fracture. The large inclusions and bi-film defects on the surface of the Silicate 2 specimen have no doubt contributed to the drop in breaking energy from 140 J (Silicate 1) to less than 100 J. Aging for 10 hrs at 530°C sharply reduced toughness to an average of 4-5 J and transitioned the fracture mode from ductile to brittle as shown in Figure 4.10 (a) and (b) for the Phos. 1 and Silicate 1 specimens, respectively. All specimens exhibited a mixture of brittle transgranular and intergranular cleavage. In areas where there was transgranular cleavage, the fracture surface exhibited characteristic linear markings as shown in Figure 4.10 (a) in the 10 hr aged Phos 1 specimen. Areas that exhibited intergranular cleavage are also noted in Figure 4.10 (a) and (b) and in some cases extend perpendicular to the fracture plane. A close inspection of the fractured interdendritic surface revealed discontinuous κ-carbide on grain boundaries in many areas.

<p style="text-align:center;">(a)   (b)</p>
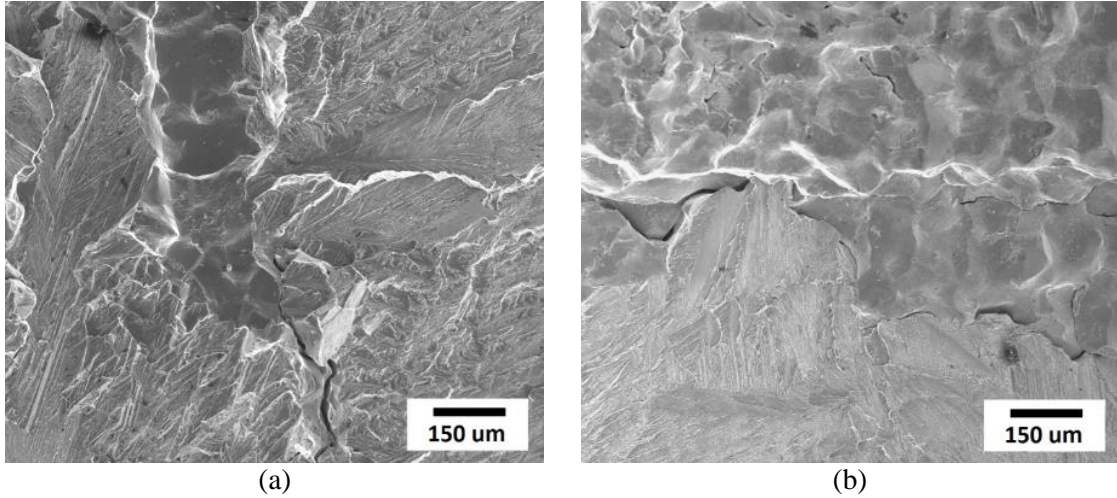
Figure 4.10: The fracture surfaces of representative Charpy bars from the (a) Phos. 1 and (b) Silicate 1 castings in the solution treated, water quenched, and aged 10 hrs at 530°C condition. Aging has transitioned the fracture mode from ductile rupture to a mixture of transgranular cleavage like fracture exhibiting characteristic linear markings along certain crystallographic directions and interdendritic cleavage along grain boundaries. (b) In areas where there was widespread interdendritic cleavage, discontinuous carbide was noted on the free surface along prior austenite boundaries.

4.5 Discussion

When transfer ladles were lined with the phosphate bonded refractory, this

resulted in what appeared to be some type of reaction between the refractory and the

molten steel and this is evident in Figure 4.2 (a and b). The silicate bonded refractory

showed no reaction with the molten steel, however, it was fairly brittle after use as shown

in Figure 4.2 (c). Previous studies by the authors show that when the high Mn and Al

austenitic steel melt is in contact with commonly used phosphate bonded refractories for

long periods of time, significant reaction occurs between the refractory and the molten

steel and this results in as much as 0.14%P reversion into the melt.[20] When the current

study is considered, the residence time between the steel and the refractory coated ladles

is rather short, less than 30 seconds. Chemical analysis of the subsequent castings in

Table 4.1 shows limited if any phosphorus pickup by the steel poured from the phosphate

coated refractory ladles. However, significant increase in silicon from 0.75 to 0.97%Si

and a slight increase in carbon, from 0.9 to 1.1%C, was noted for castings poured from

the phosphate bonded refractory ladle as shown in Table 4.1. This is consistent with the

results of the authors' previous study that shows that silicon increased from 1.56 to

2.58%Si and carbon increased from 0.9 to 1.14%C when an as-received Fe-30Mn-8.8Al-

0.9C-1.56Si0.5Mo steel was melted in contact with the phosphate bonded refractory.[20]

Phosphate bonded refractory contains almost 5% SiO_2 and this is suspected to be

the source of the increase in silicon observed for steel castings poured from the phosphate

refractory coated ladles. After experiments, a cross section of the phosphate bonded

refractory was prepared to sample the chemistry at as a function of position away from

the refractory/metal interface. A SEM image of the refractory cross section is shown in

Figure 4.11. There was no apparent reaction between steel and the refractory as observed in Figure 4.11. However, it should be noted that both the refractories were very friable and this made sample preparation and edge retention very difficult.
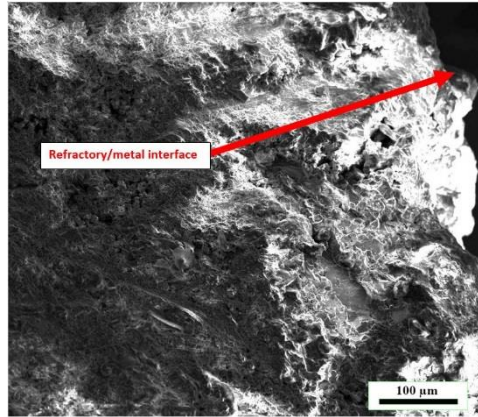
Figure 4.11: The electron micrograph of a cross section of the phosphate bonded refractory shows the interface between the refractory and molten steel.

The average chemistry of the phosphate bonded refractory was determined utilizing EDS as a function of distance away from the steel/refractory interface as shown in Figure 4.12. Phosphorus was shown to decrease from 6 to less than 2% P as a function of distance away from the interface and this shows that there was limited reduction of the phosphate binder by the molten steel during the short duration of ladling experiments. Silicon levels increased from 4 to 5.5% as the distance away from the metal interface increased to a depth of 200 μm and this may be the result of Si pickup by the molten steel. However, it should be noted that there was a large variability in the EDS chemistries and Si was shown to generally decrease with increasing distance away from the refractory metal interface. The elevated source of carbon in steels poured from the phosphate refractory coated ladle is not known, however, carbon is shown in Table 4.1 to decrease with pouring and this may be related to carbon loss during melt holding time in the furnace.
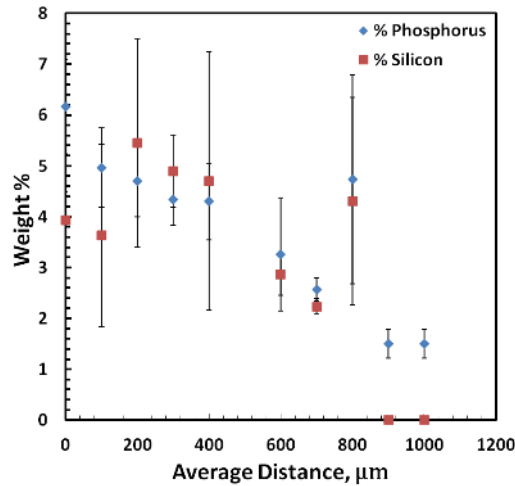
Figure 4.12: Elemental analysis of the cross section of the phosphate bonded refractory showed a general decrease in phosphorus as a function of increasing distance away from the refractory-metal interface.

Optical and SEM analysis of the as-cast microstructure showed that the major

difference between the castings was the amount of ferrite present as shown in Figure 4.3.

Ferrite in amounts up to 3% was found in the castings poured with the phosphate bonded

refractory coated ladle but was largely absent in the castings poured with the silicate

bonded refractory ladle. This is attributed to the higher levels of silicon in the Phos. 1

and Phos. 2 castings, 0.93-0.97% Si, when compared with the silicate castings, 0.74-

0.75% Si, as shown in Table 4.1. Silicon is an element that stabilizes ferrite and

increasing amounts of silicon from 0.82 to 2.24%Si promote ferrite levels of up to 16% in

the as cast condition.[21] κ-carbide was found to precipitate within the ferrite and mainly at

the ferrite/austenite interface in the as-cast microstructure as shown in Figures 4.3 and 4.5

and this is corroborated by EDS analysis in Table 4.2. This is consistent with other

researchers' reports of κ-carbide precipitation via a eutectoid reaction that occurs at the

austenite-ferrite interface and over austenite grain boundaries.[22] In the as-cast state, the

size of the matrix κ-carbide was generally greater in castings poured from the phosphate

bonded refractory coated ladle as shown in Figure 4.5 (d). This also is suspected to be

the effect of increasing silicon addition. Silicon has been shown to increase carbon activity in austenite and this results in a higher partitioning of carbon into the κ-carbide and a general increase in carbide size.[23] The presence of a phosphide eutectic was found to a small extent in all castings as shown in Figure 4.5 (d) and Table 4.2. The phosphide eutectic was found to be rich mainly in Mn, Si, and P with up to 5% C and this is consistent with previous results for a steel of similar composition.[15] After solution treatment, the amount of ferrite was greatly reduced to less than 1% in the castings poured from the phosphate bonded refractories and completely eliminated in the silicate castings as shown in Figure 4.4. Solution treatment of the Fe-30Mn-9Al-0.9C alloy above 950℃ is known to result in a fully austenitic microstructure and this greatly decreases or eliminates the amount of ferrite.[2,21,22] The phosphide eutectic was also eliminated with solution treatment and this also consistent with other researchers' results.[24]

Analysis of age hardening curves presented in Figure 4.7 show that the castings had similar solution treated hardness values of around 210 BHN. This is comparable to previously reported results by Bartlett et al. that reported the solution treated hardness around 200 BHN for a Fe-30Mn-9Al-1Si-0.9C-0.5Mo steel with less than 0.006%P.[5,25] However, the Phos. 1 castings showed slightly higher age hardening kinetics as shown in Figure 4.7 (a). This casting also showed the highest silicon and carbon contents. Increasing both carbon and silicon levels has been shown to increase the kinetics of κ-carbide precipitation and this is likely the result of higher hardening rate for the Phos. 1 casting.[5] Hardness increased to greater than 290 BHN after aging only one hour at 530℃ as shown in Figure 4.7, and then increased to greater than 375 BHN after aging for 60hrs. In figure 4.13, age hardening curves from the current study are compared to previous

results by Bartlett et al. for a nominal steel composition of Fe-30Mn-9Al-1Si-0.9C-0.5Mo with differing amounts of phosphorus.[26] Increasing levels of phosphorus from 0.006 to 0.018%P was shown to dramatically increase the kinetics of κ-carbide precipitation and thus the hardening rate.[26] The steels in the current study have a similar composition as the 0.006% P steel in Figure 4.13, however, the hardening kinetics are similar to the 0.018%P steel reported by Bartlett et al.[26]
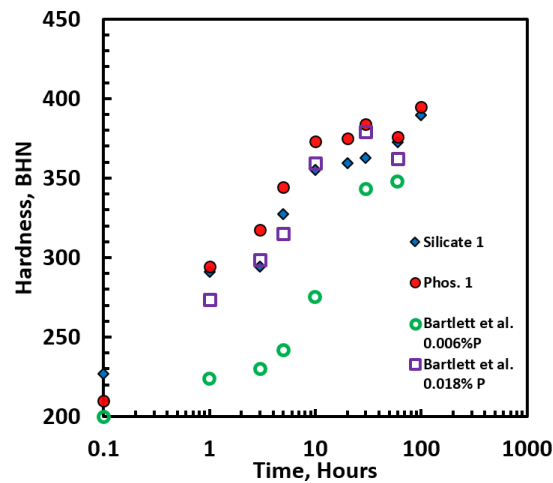
Figure 4.13: Age hardening curves at 530°C for the steels in the current study are shown with previous results by Bartlett et al. for a Fe-30Mn-9Al-1Si-0.9C-0.5Mo steel with different phosphorus contents.

The reason for the higher than expected hardening rate in the steels aged at 530°C in the current study is unknown at this time and is the subject of current investigation. Notch toughness of Fe-Mn-Al-C steels is a complex function of chemistry, heat treatment, and cleanliness. Room temperature notch toughness for the steels in the current study is shown in Figure 4.8 for specimens in the as-solution treated and aged conditions. In the solution treated condition, breaking energies ranged from 96 J for the Silicate 2 casting to 160 J for the Phos. 2 casting. These values are quite similar to a previously reported value of 124 J for a solution treated Fe-30Mn-9Al-1Si-0.9C-0.5Mo steel with low phosphorus (0.006%P).[5] In general, the castings poured from the ladle

lined with the phosphate bonded refractory were observed to have a higher average breaking energy in the solution treated condition than castings poured from the silicate bonded refractory coated ladle. This is most likely due to the increased carbon content observed in the castings poured from phosphate bonded refractory as shown in Table 4.1. In the solution treated condition, increasing the amount of carbon in solid solution from 0.9% to 1.2% has been shown to increase the dynamic fracture toughness of a Fe-30Mn-2.9Al-1Si-0.5Mo steel by 130 kJ/m^2.[27] The short range ordering of Mn-C couples in solution treated high manganese steel has been suggested by many to be the principal cause of rapid work hardening and increased plasticity in Fe-Mn-Al-C steels.[28-30] Medvedeva et al.[31] have shown that the formation of Mn-C couples in solid solution austenite is energetically favorable in high manganese steels and therefore adding solid solution carbon would increase work hardening and increase toughness. The lower breaking energy of the Silicate 2 castings in the solution treated condition is attributed to the large amount of rather course inclusions noted on the fracture surface as observed in Figure 4.9 (b). These castings were the last to be poured and represent the dirtiest metal from the remaining 20% of the furnace volume.

After aging for 10 hours at 530ºC, toughness dropped significantly from around 100 J to an average of 4 or 5 J and the hardness significantly increased to greater than 370 BHN. This behavior is consistent between the castings studied here. These results can be directly compared with previously reported results and a value of 93 J with a hardness of 300 BHN for a Fe-30Mn-9Al-1Si-0.9C-0.5Mo steel with 0.001%P that was aged for 12 hours at 530ºC.[5] The increased hardening rate and thus higher amount of κ-carbide precipitation in the current steels has resulted in substantial decrease in toughness from

what is expected based on the literature. Age hardening transitioned the fracture mode from ductile failure via nucleation and coalescence of micro-voids to a brittle, cleavage-like fracture as shown in Figures 4.9 and 4.10. Brittle fracture was both transgranular and intergranular in nature. Observations of the intergranular fracture showed that it was brittle in nature and possibly nucleated by areas of what appear to be carbide on grain boundaries. Transgranular fracture showed characteristic linear markings on cleavage facets as shown in Figure 4.10 (a). It has been shown that age hardening results in a significant reduction in work hardening and toughness in high manganese and aluminum steels.[27,32] Acselrad et al. reported a 250 MPa√m decrease in toughness in a Fe-28Mn-8.5Al-1C alloy after aging for 15hrs at 550°C and this was attributed to κ-carbide precipitation in the matrix.[32] The mechanism of the brittle cleavage fracture with aging was proposed to be the result of "slipping off" along the slip plane producing a {111} type fracture. This fracture was similar in nature to that observed in the current age hardened steels and was highlighted by characteristic linear markings on the fracture facets as shown in Figure 4.10. Acselrad et al. asserted that this fracture was facilitated by planar slip and shear strain localization in shear bands resulting from κ-carbide precipitation.[32]

4.6 Conclusion

Phosphorus pick-up from phosphate bonded refractories that are commonly used in induction melting is a problem in high manganese and aluminum steels and can result in an increase of greater than 0.14%P when steels are melted in contact with these refractories. The current study evaluated steel-refractory interactions in a nominal composition Fe-30%Mn-9%Al-0.75%Si-0.9%C-0.5%Mo steel during melt transfer operations when there is much shorter residence time for the steel to be in contact with the refractory. Results showed that when the phosphate refractory was used to coat the ladles, this resulted in only a slight increase in phosphorus content that was not statistically significant. However, Si increased from 0.74 to 0.97% when the phosphate bonded refractory was used to transfer the steel from the furnace to the molds and this may be attributed to reversion of Si from the refractory into the melt. Analysis of the resulting microstructures showed that the major difference in the as-cast structure was a higher amount of ferrite with increasing Si content. In the solution treated condition, the room temperature notch toughness was higher for the castings poured from phosphate bonded refractories, 140-160 J, and this is attributed to slightly higher carbon content. Toughness in the solution treated condition was similar to values reported from literature for almost identical compositions and processing conditions. However, the current castings showed significantly higher hardening rates when age hardened at 530ºC than what has been reported in literature for similar compositions and this is the subject of future investigations. After aging for 10 hrs at 530ºC, notch toughness decreased dramatically to an average of 4 or 5 J and this was independent of chemistry. The current

results therefore show that phosphate bonded refractories should not be used when

casting high Mn and Al steels, even during melt transfer operations.

4.7 References

1. Frommeyer, G. and Brux, U., "Microstructures and Mechanical Properties of High Strength Fe-Mn-Al-C Light-weight TRIPLEX Steels," Steel Research Int., Vol. 77, pp. 627-633 (2006).

2. Howell, R.A., Weerasooriya, T. and Van Aken, D.C., "Tensile, High Strain Rate Compression and Microstructural Evaluation of Lightweight Age Hardenable Cast Fe-30Mn-9Al-XSi-0.9C-0.5Mo Steel," AFS Trans. Vol. 117, pp. 751-763 (2009).

3. Ham, J. L., Cairns, R. E., "Manganese Joins Aluminum to Give Strong Stainless," Product Engineering, Dec, pp. 51-52 (1958).

4. Brady, G.S., Clauser, H.R., "Manganese Aluminum Steel," Materials Handbook, 11th Ed., p. 497 (1977).

5. Bartlett, L. and Van Aken, D.C., "High Manganese and Aluminum Steels for the Military and Transportation Industry," JOM, Vol. 66, No. 1 pp. 1770-1784 (2014).

6. Kayak, G. L., Met. Sc. And Heat Tr., Vol. 11, pp. 95-97 (1969).

7. Howell, R. A., Lekakh, S. L., Van Aken, D. C., Richards, V. L., AFS Transactions, Vol. 116, pp. 867-878 (2008).

8. Sato, K., Igarashi, Y., Inoue, Y., Yamazaki, T., Yamanaka, M., "Microstructure and Age Hardening in Spinodally Decomposed Austenitic Fe-Mn-Al-C Alloys," Proceedings of the International Conference on Stainless Steels (1991).

9. Ishida, K., Ohtani, H., Naoya, S., Kainuma, R., Nishizawa, T., ISIJ, Vol. 30, pp. 680-686 (1990).

10. Han, K. H., Choo, W. K., Choi, D. Y., Hong, S. P., TMS-AIME, pp. 91-106 (1987).

11. Acselrad, O., Kalashnikov, I. S., Silva, E. M., Simao, R. A., Achete, C. A., Pereira, L. C., Metallurgical and Materials Transactions A , Vol. 33A, pp. 3569-3572 (2002).

12. Ikarashi, Y., Sato, T., Yamazaki, T., Inoue, Y., and Yamanaka, M., Journal of Materials Science Letters, Vol. 11, pp. 733-735 (1992).

13. Han, K.H., Yoon, J.C., and Choo, W.K., Scripta Metallurgica, Vol. 20, pp. 33-36 (1986).

14. O. Acelrad, J. Dille, L.C. Pereira, and J. Delplancke, "Room Temperature Cleavage Fracture of FeMnAlC Steels," Met. Trans A, Vol. 35A, pp. 3863-3866 (2004).

15. Howell, R.A. and Van Aken, D.C. "Communication: Microstructural and Fracture Behavior of Phosphorus Containing Fe30Mn-9Al-1Si-0.9C-0.5Mo Alloy Steel," Metallurgical and Materials Transactions A. Vol. 46 A, No. 7 (2015) published online July 2015 DOI 10.1007/s11661-015-2971-8.

16. Medvedeva, N. I., Howell, R. A., Van Aken, D. C., & Medvedeva JE. Effect of phosphorus on cleavage fracture in κ-carbide. Phys Rev B. 2010;81(1):12105

17. Schulte, A.M., Lekakh, S.N. , Van Aken, D.C., and Richards, V.L., "Phosphorus Mitigation in Cast Lightweight Fe-Mn-Al-C Steel," AFS Trans. 118, pp. 451- 463 (2010).

18. R.A. Howell, J.M. Montgomery, and D.C. Van Aken: J. AIST, vol. 6. pp. 168-176 (2009).

19. Banerjee S. Monolithic Refractories: A Comprehensive Handbook. World Scientific; 1998.

20. Rahman, R. and Bartlett, L.N., "Steel Refractory Interactions and Elimination of Phosphorus pickup in High Mn and Al Steels," AFS Trans. 124, (2016).

21. Howell, R.A., Lekakh, S.N., Van Aken, D.C., and Richards V.L., "The Effect of Silicon Content on the Fluidity and Microstructure of Fe-Mn-Al-C Alloys," AFS Transactions 2008, Vol. 116, pp. 867-878.

22. Goretskii, G. P., Gorev, K. V., "Phase Equilibria in Fe-Mn-Al-C Alloys," Russian Met., Vol. 2, pp. 217-221 (1990).

23. L.N. Bartlett, D.C. Van Aken, J. Medvedeva, D. Isheim, N. Medvedeva, and K. Song, "An Atom Probe Study of κ-carbide Precipitation and the Effect of Silicon Addition," Met. Mater. Trans. 45A, pp. 2421-2435 (2014).

24. D. Shulik, L. Kamarash, Y. Vilchko, and P. Dzugas, "Phosphide Eutectic in a Hadfield Steel Structure," Translated from Metallovedenie I Termicheskaya Obrabotka Metallov. No. 2, pp. 2-3 (1992).

25. L. Bartlett, R.A. Howell, A. Schulte, D. Van Aken, and K. Peaslee, Proc. Materials Science and Technology Conference (Warrendale, PA: TMS, 2010), pp. 1941–1953.

26. Bartlett, L.N., Van Aken, D.C., Peaslee, K.D., and Howell R.A., "Effect of Phosphorus and Silicon on the Precipitation of κ-carbides in Fe-30%Mn-9%Al-X%Si-0.9%C-0.5%Mo Alloys," AFS Transactions 2010, Vol. 118, pp. 413-424.

27. Bartlett, L.N., and Van Aken, "Effect of Aluminum and Carbon on the Dynamic Fracture Toughness of Fe-Mn-Al-C Steels," AFS Transactions 2013, Vol. 118, pp. 511-533.

28. Y. Dastur and W. Leslie, "Mechanism of Work Hardening in Hadfield Manganese Steel," Metallurgical Transactions A, Vol. 12 pp. 749-759 (1981).

29. Bouaziz, O. and Guelton, N., "Modelling of TWIP Effect on Work-hardening," Materials Science and Engineering A Vol. 319-321 pp. 246-249 (2001).

30. Park, K., Jin, K., Han, S., Hwang, S., Choi, K., and Lee, C., "Stacking Fault Energy and Plastic Deformation of Fully Austenitic High Manganese Steels: Effect of Al addition," Materials Scinece and Engineering A Vol. 527 pp. 3651-3661 (2010).

31. Medvedeva,N.I., Park, M.S., Van Aken, D.C., and Medvedeva, J.E., "First-principles study of the Mn, Al and C distribution and their effect on the stacking fault energies in austenite," arXiv:1208.0310v1 [cond-mat.mtrl-sci], 2012.

32. O. Acelrad, J. Dille, L.C. Pereira, and J. Delplancke, "Room Temperature Cleavage Fracture of FeMnAlC Steels," Met. Trans A, Vol. 35A, pp. 3863-3866 (2004).

5. CONCLUSION

Presence of phosphorus has been a problem for high manganese and aluminum austenitic steel due to its negative impact on the mechanical properties of the steel. Recent investigations have suggested the monolithic refractory materials use in the steel making process as one of the possible external sources of phosphorus. For the investigation, a small scale laboratory and a real-time foundry experiments were done which involved melting and making of low phosphorus (0.002 to <0.006%) steels with nominal composition of 30%Mn-9%Al-0.89-1%C-1-1.56%Si-0.5Mo. In the experiment popular plastic rammable phosphate bonded monolithic refractory that is suspected as the possible source of phosphorus and castable silicate bonded monolithic refractory was used. The laboratory scale experiment showed that long contact time of 30 min between allowed the remelted steel to react with the phosphate bonded monolithic refractory and pick-up more than 0.14% P. The microstructure of the as-cast steel was found to contain a large amount of phosphide eutectic phase with heavy grain boundary k-carbide precipitation. Comparatively little reaction took place in case of silicate bonded monolithic refractory and no change in phosphorus content was observed. The real-time foundry melt transfer operation experiment showed insignificant increase in phosphate content by the steel poured from phosphate bonded monolithic refractory lined ladle due to short contact period. In both the experiments, all steels were found to have slightly increased C and Si content after reacting with phosphate Thus the results of both the studies indicate that high manganese and aluminum steels can pick-up phosphorus by reacting with the phosphate bonded monolithic refractory at steel making temperatures. The results suggest that high manganese and aluminum steel making facilities should not

use phosphate bonded monolithic refractories for melting or melt handling operations.

These refractories should be replaced by silicate bonded refractories.

REFERENCES

1. Mizumoto M, Sasaki S, Ohgai T, Kagawa A. Development of new additive for grain refinement of austenitic stainless steel. Int J Cast Met Res. 2008;21(1-4):49-55. doi:10.1179/136404608X361657.

2. Kim H, Suh D-W, Kim NJ, et al. Fe–Al–Mn–C lightweight structural alloys: a review on the microstructures and mechanical properties. Sci Technol Adv Mater. 2013;14(1):14205. doi:10.1088/1468-6996/14/1/014205.

3. Ham J, Jr RC. Manganese joins aluminum to give strong stainless. Prod Eng. 1958.

4. Frommeyer G, Bruex U. Microstructures and mechanical properties of high-strength Fe-Mn-Al-C light-weight TRIPLEX steels. Steel Res Int. 2006;77:627-633.

5. Bartlett LN, Aken DC Van, Lekakh S, Peaslee KD. Mechanical Properties of Cerium-Treated Fe-Mn-Al-C Steel Castings Copyright 2011 American Foundry Society. AFS Trans Foundry Soc. 2011;119:545.

6. Bartlett L, Aken D Van. High Manganese and Aluminum Steels for the Military and Transportation Industry. JOM. 2014;66(9):1770-1784.

7. Sato, K., Igarashi, Y., Inoue, Y., Yamazaki, T., & Yamanaka M. Microstructure and Age Hardening in Spinodally Decomposed Austenitic Fe--Mn--Al--C Alloys. Stainl Steels. 1991;1:503-509.

8. Howell RA, Weerasooriya T, Aken DC Van. Tensile , High Strain Rate Compression and Microstructural Evaluation of Lightweight Age Hardenable Cast Fe-30Mn-9Al-XSi-0 . 9C-0 . 5Mo Steel. Trans Am Foundry Soc. 2009;117(09-):751-764.

9. Schindler H. Estimation of the dynamic JR-curve from a single impact bending test. ECF11, Poitiers 1996. 2013.

10. Prodhan A, Charkrabarti AK. A Study on Cast Fe-Mn-Al-Si-C Alloys. AFS Trans. 1990;37:35-46.

11. Goretskii G, Gorev K. Phase Equilibria in the Fe--Mn--Al--C Alloys. Izv Akad Nauk SSSR, Met. 1990.

12. McLean, D., Northcott L. Micro examination and electrode-potential measurements of temper brittle steels. J Iron Steel Inst. 1948;158:169-177.

13. Howell R, Aken D Van. Microstructural and Fracture Behavior of Phosphorus-Containing Fe-30Mn-9Al-1Si-0.9 C-0.5 Mo Alloy Steel. Metall Mater Trans A. 2015;46(8):3309-3316.

14. Rahman R, Bartlett LN. Steel-Refractory Interactions and Phosphorus Pickup during Melting of High Manganese and Aluminum Steels. In: Minneapolis, MN: AFS Transactions-American Foundry Society; 2016.

15. Howell, R.A., Lekakh, S.N., Medvedeva, J.E., Medvedeva, N.I., and Van Aken DC. Phosphorus and Thermal Processing Effects on Charpy V Notch Impact Toughness of Lightweight Fe 30Mn 9Al 1Si 0.9 C 0.5 Mo. Met Trans A, (submitted Publ.

16. Medvedeva, N. I., Howell, R. A., Van Aken, D. C., & Medvedeva JE. Effect of phosphorus on cleavage fracture in κ-carbide. Phys Rev B. 2010;81(1):12105.

17. Howell R, Lekakh S, Aken D, Richards V. The Effect of Silicon Content on the Fluidity and Microstructure of Fe-Mn-Al-C Alloys. Transactions of the American Foundrymen's Society 2008;(116):867-878.

18. Schulte A, Lekakh S, Aken D Van, Richards V. Phosphorus Mitigation in Cast Lightweight Fe-Mn-Al-C Steel (10-057). Transactions of the American Foundrymen's Society. 2010;118:451.

19. Howell RA, Montgomery JS, Van Aken DC. Advancements in Steel for Weight Reduction of P900 Armor Plate. 2009;6:168-176.

20. SUTCLIFFE N. Slag/refractory and metal/refractory interactions during the production of stainless steels. In: Cape Town: The South African Institute of Mining and Metallurgy; 2004.

21. President Obama Announces Historic 54.5 Mpg Fuel Efficiency Standard.; 2011..

22. Burnham T, Hadfield R. Special Steels. 1933.

23. Hadfield R. Manganese Steel. Oliver and Boyd ltd., Edinburgh, UK; 1956.

24. Stephens JR. New alloys to conserve critical elements. In: ; 1978.

25. Banerji S. An Update on Fe-Mn-Al Steels. In Proceedings of the Workshop on ''Conservation and Substitution Technology for Critical Materials'', Vanderbilt University, Nashville, Tennessee. 1981

26. Contingency Plans for Chromium Utilization. Natl Mater Advis Board, Natl Acad Sci. 1978.

27. Lin CL, Chao CG, Bor HY, Liu TF. Relationship between Microstructures and Tensile Properties of an Fe-30Mn-8.5Al-2.0C Alloy. Mater Trans. 2010;51(6):1084-1088. doi:10.2320/matertrans.M2010013.

28. Yoo JD, Park K-T. Microband-induced plasticity in a high Mn–Al–C light steel. Mater Sci Eng A. 2008;496(1):417-424. doi:10.1016/j.msea.2008.05.042.

29. Chang SC, Hsiau YH, Jahn MT. Tensile and fatigue properties of Fe-Mn-Al-C alloys. J Mater Sci. 1989;24(3):1117-1120. doi:10.1007/BF01148807.

30. James P. PRECIPITATION OF THE CARBIDE--FEMN--3 ALC IN AN IRON-ALUMINIUM ALLOY. J Iron Steel Inst. 1969:54-57.

31. Sato K, Tagawa K, Inoue Y. Modulated structure and magnetic properties of age-hardenable Fe-Mn-Al-C alloys. Metall Mater Trans A. 1990;21(1):5-11.

32. Kalashnikov IS, Acselrad O, Shalkevich a., Chumakova LD, Pereira LC. Heat treatment and thermal stability of FeMnAlC alloys. J Mater Process Technol. 2003;136(1-3):72-79. doi:10.1016/S0924-0136(02)00937-8.

33. Kimura, Y., Hayashi, K., Handa, K., & Mishima Y. Microstructure control and ductility improvement of the two-phase γ-Fe/κ-(Fe, Mn) 3 AlC alloys in the Fe–Mn–Al–C quaternary system. Mater Sci Eng A. 2002;329:680-685.

34. Howell R, Weerasooriya T, Van Aken D. Tensile, High Strain Rate Compression and Microstructural Evaluation of Lightweight Age Hardenable Cast Fe-30Mn-9Al-XSi-0.9C-0.5Mo SteelTensile, High Strain Rate Compression and Microstructural Evaluation of Lightweight Age Hardenable Cast Fe-30Mn-9Al-XSi. Int J Met. 2010;4(1).

35. Kayak G. Fe− Mn− Al precipitation-hardening austenitic alloys. Met Sci Heat Treat. 1969.

36. Acselrad O, Simao R, Pereira L. Phase transformations in FeMnAlC austenitic steels with Si addition. Metallurgical and Materials Transactions A. 2002;33:3569-3572.

37. Acselrad O, Pereira L, Amaral M do. Processing Conditions, Microstructure and Strength of an Austenitic FeMnAlC alloy. Process Prop Appl Met Ceram Mater. 1992;2:829-834.

38. Sutou Y, Kamiya N, Umino R, Ohnuma I, Ishida K. High-strength Fe-20Mn-Al-C-based alloys with low density. ISIJ Int. 2010.

39. Bartlett L, Dash A, Van Aken D, Richards V, Peaslee K. DYNAMIC FRACTURE TOUGHNESS OF HIGH STRENGTH CAST STEELS. Int J Met. 2013;7(4):17-33.

40. Han KH, Choo WK. Phase decomposition of rapidly solidified Fe-Mn-Al-C austenitic alloys. Metall Trans A. 1989;20(2):205-214. doi:10.1007/BF02670246.

41. Ishida K, Ohtani H, Satoh N, Kainuma R, Nishizawa T. Phase equilibria in Fe-Mn-Al-C alloys. ISIJ Int. 1990.

42. Prodhan, A., Chakrabarti AK. A Study on Caste Fe-Mn-Al-Si-C Alloys. AFS Trans. 1990;37:35-46.

43. Howell R. Microstructural influence on dynamic properties of age hardenable FeMnAl alloys (No. ARL-RP-0321). ARMY Res LAB ABERDEEN PROVING Gr MD. 2011.

44. Krivonogov, G. S., Alekseenko, M. F., & Soloveva GG. Phase Transformation Kinetics of Steel 9 G 28 Yu 9 MVB. Phys Met Met. 1975;39(4):86-92.

45. Cheng W-C, Lin H-Y. The precipitation of FCC phase from BCC matrix in an Fe–Mn–Al alloy. Mater Sci Eng A. 2002;323(1):462-466. doi:10.1016/S0921-5093(01)01498-8.

46. Fordyce W. A History of Coal, Coke, Coalfields and Iron Manufacture in Northern England.; 1860.

47. Clayton JQ, Knott JF. Phosphorus segregation in austenite in Ni–Cr and Ni–Cr–Mn steels.

48. Bartlett L, Aken D Van, Peaslee K, Howell R. Effect of Phosphorus and Silicon on the Precipitation of K-Carbides in Fe-30% Mn-9% Al-X% Si-0.9% C-0.5% Mo Alloys (10-069). Transactions of the American Foundrymen's Society. 2010;118:413.

49. Acselrad O, Pereira LC, Dille J, Delplancke J-L. Room-temperature cleavage fracture of FeMnAlC steels. Metall Mater Trans A. 2004;35(12):3863-3866. doi:10.1007/s11661-004-0292-4.

50. Cramb A. Secondary steelmaking and casting: the basis for control of steel properties and quality. Scand J Metall. 1997;26:2-7. http://cat.inist.fr/?aModele=afficheN&cpsidt=2246019. Accessed August 1, 2016.

51. Poirier J. A review: influence of refractories on steel quality. Metall Res Technol. 2015;112(4):410.

52. Karakus M, Moore R. Cathodoluminescence (CL) microscopy application to refractories and slags. J Miner Mater Charact. 2002;1(1):11.

53. Volume A. 15.01 Refractories; Activated Carbon.

54. Schacht CA. Refractories Handbook. Marcel Dekker; 2004.

55. Caniglia S, Barna G. Handbook of Industrial Refractories Technology: Principles, Types, Properties and Applications.; 1992.

56. Lee W, Rainforth M. Ceramic Microstructures: Property Control by Processing.; 1994.

57. Poirier J. A review: influence of refractories on steel quality. Met Res Technol. 2015;112(410). doi:10.1051/metal/2015028.

58. Pickering GDDB. Carbon-MgO reactions in BOF refractories. AMER CERAM SOC BULL . 1971;50(7).

59. BRABIE V. A study on the mechanism of reaction between refractory materials and aluminium deoxidised molten steel. Steel Res. 68(2):54-60.

60. Watanabe A, Takahashi H, Nakatani F. Mechanism of Dense Magnesia Layer Formation near the Surface of Magnesia-Carbon Brick. J Am Ceram Soc. 1986;69(9):C-213-C-214. doi:10.1111/j.1151-2916.1986.tb07482.x.

61. Hauck, F., Markert, J., & Potschke J. Interactions Between Refractories and Melts at High Temperature Processes, Advances in Transport Processes in Metallurgical Systems. Elsevier Sci B V. 1992:113-164.

62. Lee WE, Zhang S. Melt corrosion of oxide and oxide–carbon refractories.

63. Banerjee S. Monolithic Refractories: A Comprehensive Handbook. World Scientific; 1998.

64. Garbers-Craig A. Presidential address: How cool are refractory materials? J South African Inst Min Metall African Inst Min Metall. 2008;108.

65. KINGERY, W.D., BOWEN, H.K. and UHLMAN DR. Introduction to Ceramics. 2dn ed. New York: Wiley-Interscience; 1960.

66. Rigaud, M. A., & Landy RA. Pneumatic Steelmaking.: Refractories. Iron Steel Soc. 1996.

67. Krebs R. Unshaped Refractory Products. CRC Press Fr. 2004;178:287.

68. Decker J. Phosphate bonded monolithic refractory materials with improved hot strengths as a potential replacement for phosphate bonded bricks. Mater Sci Forum. 2011.

69. Thrower S, Criss G, Moniot D. Monolithic refractories. US Pat 3,998,648. 1976.

70. Kuang JP, Harding RA, Campbell J. Investigation into refractories as crucible and mould materials for melting and casting gamma-TiAl alloys. Mater Sci Technol. 2000;16(9):1007-1016.